Engineering Combinatorial Microenvironments for Structural and Functional Maturation of Human Stem Cell-Derived Cardiomyocytes

Daniel Carson

A thesis submitted in partial fulfillment of the requirements for the degree of

Master of Science in Bioengineering

University of Washington

2013

Committee:

Deok-Ho Kim

Candan Tamerler

Program Authorized to Offer Degree:

College of Engineering

University of Washington

Abstract

Engineering Combinatorial Microenvironments for Structural and Functional Maturation of Human Stem Cell-Derived Cardiomyocytes

Daniel Carson

Chair of the Supervisory Committee:

Dr. Deok-Ho Kim

Bioengineering

As cardiovascular disease remains to be the leading cause of death worldwide, cardiac regenerative medicine aims to apply design methods to develop functional cardiac tissue for directed therapy as well as *in* vitro screening assays. Research in this area has shown varying degrees of success, but fully functional cardiac tissue remains to be achieved. This short-coming is due to failures in mimicking native heart tissue *in vitro*. The extracellular matrix (ECM) of the heart is a complex structure responsible for both biochemical and mechanical cues to the surrounding myocardium. Past research has relied heavily on the use of native biochemical signals of the ECM to influence cardiomyocyte function, but the mechanical signals of heart ECM have been less studied. The ECM of the heart is made up of aligned collagen fibers as well as other important proteins in the basement membrane responsible for cell-cell and cell-ECM interactions. The nanoscale collagen fibers have been shown to play a major role in the

structural architecture of the overlying macroscopic myocardium. Advancements in nanofabrication techniques have made it possible to study the effect of substrate nanotopography on cardiomyocyte structure and function. The proteins of the basement membrane including laminin and fibronectin have been shown to strongly influence the adhesion of cardiomyocytes through integrin interactions. Recently, a specific repeating amino acid sequence, Arg-Gly-Asp (RGD), found in many native adhesion proteins, has been shown to promote cell adhesion *in vitro*[1,2].

Here we present a platform in which we are able to study the effect of nanoscale structural cues as well as ECM biochemical signals on maturation of human pluripotent stem cell-derived cardiomyocytes (hPSC-CMs). Using a customized 4 x 4 island nanopatterned substrate, nanogroove widths ranging from 350nm to 2000nm were investigated. We also present the synthesis and incorporation of bifunctionalized peptide, PUA binding peptide – RGD (PUABP-RGD) into the platform to further study the effect of native ECM-like biochemical cues on the structural maturation of hPSC-CMs.

Acknowledgments

I would like to start by thanking by advisor Dr. Deok-Ho Kim who has mentored me both as an undergraduate and a graduate student. I joined Dr. Kim's lab when I was a junior in the bioengineering department and went on to complete my senior capstone with Dr. Kim. I would like to highlight Dr. Kim's ambition and the excitement he displays towards his research and the students in his lab. In my first interview with him, before joining the lab, I could see how passionate he was about his work which immediately resonated with me and made me excited about the prospect of pursuing my research interests under his guidance. Over the course of my time in the lab I have experienced setbacks and successes, but Dr. Kim always showed his support. His willingness to discuss ideas with me and provide advice for my projects will be fondly remembered. I am deeply appreciative to Dr. Kim for providing me with the opportunity to participate in cutting edge research.

I would also like to thank Dr. Candan Tamerler who served on my thesis committee. As a faculty member of the Material Science & Engineering department I was fortunate enough to collaborate with her lab for my thesis work. Marketa, a post-doctoral fellow (Tamerler Lab), was an integral member of our collaborative efforts. I would also like to thank Dr. Mike Regnier who co-advised my senior capstone project as an undergraduate student and continued to provide his support during my graduate studies. Next, I would like to acknowledge Dr. Chuck Murry and Dr. Michael Laflamme for providing their lab resources in collaborative projects.

Xiulan Yang, post-doctoral fellow (Murry Lab), was an excellent colleague to collaborate with for my thesis work. She was always upbeat and supportive of my work

and I am truly thankful for the opportunity to work alongside her. Hee Seok Yang and Hyun Jung Lee, former post-doctoral fellows of the Kim lab, were two of the first members I met and worked with in the Kim lab. I would specifically like to acknowledge their patience and willingness to help me learn lab techniques as a new member of the lab.

Alex Jiao, a PhD student (Kim Lab), deserves a special thanks as he was my immediate mentor upon joining Dr. Kim's lab. His support and guidance during my undergraduate and graduate studies were instrumental in achieving my research goals. I am extremely appreciative to have worked with such a driven scientist for close to 3 years and am glad to have developed a close friendship. Jesse Macadangdang, Hyok Yoo, and Jonathan Tsui are 3 other PhD students in the Kim lab that were very supportive of my research goals and were always available with advice or help. I would also like to thank the Department of Bioengineering at the University of Washington who gave me the chance to study bioengineering at the ungraduated and graduate levels.

Finally, I would like to acknowledge my family and friends who have been the core of my support network, not only during my time at the University of Washington, but also throughout my life. My mother, Connie, and my father, Doug, have always been there for me, regardless of the situation. Their overwhelming support of my academic pursuits will always be remembered. I would also like to acknowledge my grandparents David, Marilyn, and Nan who continue to provide me with support and positive influence. My sister, Meghan, and my brother, Christopher, are also huge parts of my life. Finally, I would like to acknowledge the Kanady family (Lynn, Tim, Shane, and Paige) who I consider my second family. Their massive support of me has been so important to my personal and academic development.

Table of Contents

List of Figures

CHAPTER 1: INTRODUCTION

1.1 *Motivation*

One of the primary goal of cardiac tissue engineering is to repair damaged or diseased myocardium. Success in accomplishing this goal can be evaluated by improvements in heart function, mainly by assessing the ability of the heart to pump blood. Tissue engineering efforts have aimed to achieve this goal by facilitating the assembly of cells in to functional cardiac tissues. In the past, research have attempted to reach this goal through the use of immature rodent cardiac cells. This approach was very common because they are readily available, robust, and comprehensively studied. However, recently researchers have come to realize the major limitations associated with rodent cardiomyocytes when aiming to develop functional tissues for therapy and modeling. The major limitation with this cell type stems from the source itself. The ability to draw meaningful conclusions from modeling or therapeutic studies are limited because of physiological differences between animal and human cells.

This understanding has led to recent advancements in directed differentiation of human pluripotent stem cell-derived cardiomyocytes (hPSC-CMs)[12-13]. As these cell lines have become more established, the potential for hPSC-CM in cardiac tissue engineering has been greater. Most importantly, the successful derivation of cardiomycyotes of human origin creates the opportunity for more accurate modeling of cardiac diseases as well as improved benefits in therapeutic applications.

Although promising advancements have made using hPSC-CMs, success has been ultimately limited by the ability to engineering these cells to present phenotype similar to adult human cardiomyocytes. The three main goals of cardiac tissue

engineering focus on engineering functional myocardium for directed therapy, drug screening, and disease modeling. The transition to hPSC-CMs as certainly progressed the field towards these three goals, but the remaining issue of developing structurally and functionally mature human cardiac cells prevents ultimate success. First, in therapeutic applications (repairing damaged myocardium) a mature cardiac cell would be desired to ensure optimal electromechanical coupling with host tissue while also reducing the risk of arrhythmia. Second, in a drug screening setting, it a cardiac cell that closely resembles native myocardium (mature cell) would provide the most accurate effects of a potential drug. Finally, in a disease modeling setting, it would be expected that attempting to investigate a diseased cell type that was not representative of native pathological environment would hinder the effectiveness of the study. Therefore, current and ongoing lab efforts have focused on structurally and functionally maturing hPSC-CMs.

1.2 *Background*

1.2.1 *Heart Disease/Myocardial Infarction*

The heart is one of the most complex and vital organs in the entire human body. It is essentially a mechanical pump responsible for shuttling blood (oxygen) to regions all over the body. While the intricately structured organ has a number of unique functional properties it also has a variety of ways it can be damaged. A less functional or underperforming heart can have grave short and long term impacts. It is therefore essential to monitor the health and function of the heart while also investigating methods to fix it when it becomes damaged.

One such injury a heart can sustain is a myocardial infarction. While the heart is responsible for pumping blood to vasculature throughout the body, there are also vessels

that surround the heart and provide oxygen to allow the heart to function. A myocardial infarction occurs when a vessel supplying a portion of the heart becomes occluded. Plaque buildups and other blockages are often responsible for the occlusions and can either be acute (short term occlusion that passes) or chronic (permanent occlusion). Occlusion of coronary vessels prevents oxygen from reaching the targeted cardiac tissue. The lack of oxygen then leads to necrosis of the supplied myocardial tissue. Since the heart has a very limited capacity to repair itself (less than 1% cardiomyocytes proliferate after age of 25) the damaged tissue is replaced by less functional scar tissue[3]. The subsequent fibrosis of the ischemic region leads to large scale remodeling of the heart muscle and a decrease of long term function. This presents a major problem to individuals suffering a heart attack because the decreased function reduces quality of life and can ultimately lead to total heart failure. Although a myocardial infarction event can be fatal, improvements in emergency medical care have substantially increased initial survival rates. This creates an unmet need to devise solutions to the long term effects posed by myocardial infarctions.

Myocardial infarctions have become the leading cause of death in the United States and other industrialized nations worldwide. It has been estimated that 450,000 people die each year from coronary heart disease[4]. As of 2006, it was reported that 17,600,000 people had experienced a heart attack; with initial survival rates reaching approximately 95%, this suggests that many of the annual deaths related to coronary heart disease arise from long term complications and heart failure[5]. The statistics present clear evidence of a growing problem worldwide and the need to address potential therapeutic treatments. The best current approach to MI is preventative treatment which

includes a healthy diet, exercise, and no smoking. However, it is also necessary to develop solutions for the patients who have already experienced a heart attack. Current treatment options include complicated drug regimens and invasive interventions. It is clear that there is room for improvement when assessing treatment options for patients who have experienced a myocardial infarction.

Many of the current clinical treatments for patients presenting with a myocardial infarction are heavily dependent on the time between the attack and coming to the clinic. The first step a physician will take when treating a patient that has suffered a myocardial infarction is to limit the extent of the infarction by restoring oxygen supply to the ischemic myocardium. It has been noted that variations on infarction size and gravity among patients may be partially attributed to the extent of collateral coronary circulation each individual has. Regardless, the immediate treatment for patients treated within the first several hours is thrombolytic therapy in attempt remove the coronary blockage[6]. The most common thrombolytic medication used is tissue plasminogen activator (tPA)[6]. The advantage of using thrombolytic medications to remove blockages is that is circumvents the immediate need for invasive surgery. However, in cases where thrombolytic therapy is ineffective percutaneous coronary intervention techniques can be used. Angiography is used to display the extent of the coronary blockage which is then followed by the minimally invasive catheter removal of the blockage[6]. The advantage of mechanical removal of coronary blockages is the improved control in the removal process. However, one major risk associated with catheter based interventions is the potential embolization of the blockage. Although coronary vasculature primarily serves heart muscle, an embolism has the potential to navigate its way up to the brain causing a stroke. In

extreme cases, where the above techniques are ineffective, coronary bypass graft surgery can be performed. This is a major invasive surgery in which vessels are resected from other areas of the body and grafted to the heart to reestablish circulation to the ischemic area of the myocardium. Coronary bypass graft surgery is never the first choice as the risk associated with major open heart surgery is much higher.

The treatments described above related to the emergency care provided to patients within the first 12 hours after a heart attack. Due to the drastic improvements with these treatments, as mentioned previously, the initial survival rates of patients has increased dramatically. Although the emergency treatments listed above provide temporary relief to patients, long term effects of the damaged myocardium presents the largest area of research for therapeutic improvements. The replacement of diseased myocardium with fibrotic scar tissue initiates a detrimental restructuring of the heart muscle. As scar tissue does not possess the unique electrical and mechanical characteristics of native myocardium, normal cardiac function is interrupted. Over time ventricular wall dimensions begin to change to compensate for the ischemic area. The compensation initiated to generate normal cardiac output puts much higher stress on the heart which can ultimately to total heart failure.

Therefore, there are treatments associated with the long term effects of a myocardial infarction, but are often invasive and risky. Aside from lifelong drug regimens used to prevent future coronary occlusions the main treatments for long term effects of MI include whole heart transplants and implantation of ventricular assist devices. One of the clear disadvantages with these treatment options is the invasive nature of the surgery. Both whole heart transplants and ventricular assist device implantation require open heart

surgery which has the inherent risks associated with all major surgeries. Whole heart transplants have many other limitations including limited availability of viable hearts and the selection process a patient has to go through to be considered eligible. If a patient does qualify for a heart transplant the major risk becomes successful retention by the host. Ventricular assist devices are another treatment option containing a similar risk as a whole heart transplant. Implantation will elicit a host immune response as the material composing the ventricular assist device is foreign to the native environment. These treatments involve taking medication for immune suppression. Along with the immune response, ventricular assist devices are not permanent solutions as the devices have a limited lifespan. The limitations associated with current available MI treatments have created strong motivation for scientists, specifically cardiac tissue engineers, to investigate novel techniques to overcome current shortcomings. Other diseases that result in impaired cardiac function include hypertensive heart disease, valvular heart disease, congenital heart defects, and cardiomyopathy, the causes of which range broadly from genetic mutations and metabolic disorders to infectious disease and environmental toxins. It is important to note that cardiac tissue engineering efforts aim to repair impaired heart function as a result of ischemic injuries and other diseases mentioned above.

1.2.2 *Drug Screening*

In addition to therapeutic applications for damaged cardiac tissue, engineered functional tissue can be used *in vitro* as a platform for drug screening. Current standards for cardiotoxicity testing, during drug development, rely heavily on animal testing. Successful

development of native-like heart tissue *in vitro* could substantially alter the foundation of drug screening for pharmaceutical companies. An *in vitro* cardiac tissue platform could improve on current standards in drug screening by providing a low cost and high-throughput alternative to animal testing.

1.2.3 *Disease Modeling*

Cardiac disease modeling is another potential application for *in vitro* engineered cardiac tissue. Again, current standards rely on genetic manipulation in animal models to study heart diseases such as dilated cardiomyopathy and hypertrophic cardiomyopathy. The current standard presents a high cost and low throughput means of studying heart related diseases. The ability to establish a platform in which *in vitro* engineered cardiac tissues can mimic *in vivo* diseased cardiac tissue would provide a promising alternative to current standard which could lower cost and increase throughput of such studies.

1.2.4 *Cardiac differentiation using pluripotent stem cell-derived cardiomyocytes*

A number of cell lines have been studied in relation cardiac tissue engineering including neonatal rat ventricular myocytes (NRVM) and cardiosphere-derived cells (CDC), but each has possessed key limitations inhibiting researchers to achieve an ideal engineered cardiac tissue. Human pluripotent stem cell-derived cardiomyocytes have emerged as an extremely promising cell source as they possess unique characteristic that benefit the field of regenerative medicine. These characteristics include an essentially limitless cell source, a more physiologically relevant cell type, and the potential for patient specific therapies or disease modeling.

Two specific sources for stem cell-derived cardiomyocyte cell lines have recently garnered much attention as differentiation methods have improved; Human embryonic stem cell-derived cardiomyocytes (hESC-CM's)[12] and human induced pluripotent stem cell-derived cardiomyocytes (hiPSC-CMs)[13]. Embryonic stem cell are obtained from the inner cell mass of the blastocyst during embryonic development. As expected, certain ethical dilemmas become present when discussing embryonic derived stem cells. Induced pluripotent stem cells provide an alternative to the more controversial ESC's because they are derived from somatic cells. IPSC's are obtained by reprogramming of "terminally" differentiated somatic cells back to the pluripotent stem cell stage by induction with a variety of factors[13]. Once at the pluripotent stem cell stage, both hESCs and hiPSCs follow similar differentiation protocols (**Figure 1**). The undifferentiated stem cells are serial induced with activin A and bone morphogenetic protein-4 (BMP-4) to lead to beat cardiomyocytes[12-13].

1.2.5 *Stem Cell-Derived Cardiomyocyte Based Therapies*

Recently, many studies have investigated stem cell-derived cardiomyocyte based therapies[7-10]. Once such study was conducted by Shiba, Yuji; Fernandes, Sarah *et al.*[14] which looked at the injection of human embryonic-stem-cell-derived cardiomyocytes into guinea pick hearts post-MI. A unique aspect of the study was the generation of GCaMP3-+-hESC-CM's as the cell source. These included an encoded fluorescent calcium sensor which allowed for fluorescent imaging *in* vivo. Prior to the study critical limitations of stem cell injection approaches had not been addressed. These limitations included risk of

transplanted cells causing arrhythmias and the ability of the transplanted cells to electrically couple with host tissue.

The major findings from the paper showed results supporting hESC-CM's as arrhythmia suppressors as well as showing the ability of the target cells to electrically couple. The hESC-CM group showed reduced spontaneous ventricular tachycardia percentage 28 days post-MI and no sustained ventricular tachycardia compared to control groups. The next finding showed 100% of visible grafts showed 1:1 synchronized Ca2+ fluorescence transients with host ECG at day 14 with uninjured hearts. Following cryoinjury (inducing chronic MI), at Day 14 and 28, electrical coupling was observed. Studies indicated 1:1 host-graft coupling in approximately 60% of hearts at both time points. Although electrical coupling was smaller for the infarct model the partial coupling observed is promising for future experiments related to this technique. Although the major findings support hESC-CM's as potential cell source for therapeutic treatment, the study also highlighted limitations of the cell injection technique as a whole. A major limitation associated with all cell injection techniques regards cell retention upon delivery. As the basic concept of isolated cell injection involves dispersal of target cells into the epicardium, most cells wash away prior to grafting with host tissue.

Aside from technical limitations associated with stem cell based therapies, the findings of such studies elucidate the limits of restored heart function as the cardiomyocytes used remain phenotypically immature compared to host cardiomyocytes. Several studies have aimed at developing cardiac patches to overcome technical limitations of cell based therapies, but the main limitation associated with all studies in the

field centers around improved maturation of stem cell-derived cardiomyocytes towards native cardiomyocyte phenotypes[10,15-18].

1.2.6 *hPSC-CM Maturation*

As current clinical approaches leave much room for improvement, research groups have investigated novel methods to use hPSC-CMs. However, as mentioned, the inability to produce mature hPSC-CMs has made it necessary to find methods to influence cardiac cells towards adult phenotypes.

As a cardiac cell progresses from an immature to mature phenotype a number of complex structural and functional changes occur. One of the main factors considered for structural maturation comes from morphological changes in cardiac cells. Physiological hypertrophy is important as it is associated with action potential propagation and contractile force[50]. Shape should be considered as an important factor; immature cardiac cells display a much more round morphology in comparison to mature cardiac cells that appear rectangular and elongation. The shape of the cell can also influences the kinetics of impulse propagation as well as contraction force and directionality.

Sarcomeres are considered to the unit that directs contractions of cardiac cells. Therefore, it is important to consider the presence and structure of sarcomeres in hPSC-CMs when assessing structural maturity. Gene expression of sarcomere proteins has been shown in immature hPSC-CMs and thus has made evaluation of sarcomere structure as an essential mechanism of determining maturity[51,52]. As cardiac cells mature sarcomeres become more organized along myofibrils and sarcomere length increases to promote more forceful contractions.

Functional maturity of hPSC-CMs is predominantly evaluated through contractility and calcium handling. A number of different approaches have been investigated to measure and assess hPSC-CM contractile force[7,27]. Although, the methods remain imperfect, comparison to contractile force of mature cardiac cells shows 100+ fold differences[27]. The ability for a cardiomyocyte to generate force is functionally essential to yield a mature phenotype. Calcium handling has been widely reported as a key functional endpoint of hPSC-CM maturity. The degree to which a cardiac cell matures corresponds to how quickly it is able to turn over calcium stores. Groups have mainly focused on expression of key calcium related genes including calsequestrin or phospholambam[53]. They have gone on to investigate calcium transient amplitude, upstroke velocity, and transient decay as mechanisms to evaluate maturity of hPSC-CMs. The above mentioned characteristics have been widely investigated in regards to hPSC-CM maturity, but they do not represent all means of determining cardiomyocyte maturity. Other key indicators include: myofibrillar isoform switch[55], appearance of transverse tubules[56, 57], gap junction formation and localization[58], metabolic changes[59], multinucleation[39], cardiac related gene expression[60], and responses to calcium and beta-adrenergic stimulation[61].

1.2.7 *Current Methods for Maturation of hPSC-CMs*

The most common efforts in the past to mature hPSC-CMs *in vitro* involved application of biochemical signals to cardiac cultures. This includes adrenergic receptor agonists, triiodothyronine, insulin-like growth factor I, microRNA modification. These factors have also been used in conjunction with prolonged cultures (100+ days) to reach fractions of

adult cardiomyocyte phenotype. Within the last decade cardiac tissue engineering has transitioned towards integration of native-like myocardial environmental characteristics to mature cardiomyocytes.

Although mimicking native tissue function *in vitro* will theoretically promote drastically improved cardiomyocyte maturation, the ideal process by which this can be achieved is still far from being achieved. As mentioned, from a therapeutic standpoint immature cells or tissue that are implanted into the injury site cannot properly integrate with the surrounding native tissue. Accurate drug screening and disease modeling studies cannot be performed *in vitro* with cardiac tissue which does not represent native myocardium. Therefore, it is essential to create an environment *in vitro* that mimics the native environment of the heart as closely as possible.

The anatomical function of the heart displays a unique method of contraction that requires communication between adjacent cells and an overall structure that helps promote directional and synchronous contractions. The correct directionality of contraction is essential in the heart to ensure that movement of blood is efficient and is pushed to the correct location. As the heart contracts from the apex upwards, it is evident that the myocardium orients itself to assist in the propagation of the contraction. The directional and synchronous contractile properties of the heart are a result of the unique structural, electrical, biochemical, and mechanical environment. Many of these unique environmental characteristics can be attributed to the underlying extracellular matrix (ECM).

The ECM proteins provide structural cues for cardiac cells and are essential for normal tissue function as they coordinate mechanical and biochemical factors

surrounding the native myocardium[19, 20]. The extracellular matrix of the heart is made up of fibrillar collagens, basement membrane components, and proteoglycans. Collagens type I and III are the main constituents of fibrillar ECM in the heart and allow for the efficient propagation of cardiomyocyte force production and aid in the overall ventricular pump function[21]. The basement membrane, on the other hand, is composed of a number of proteins including laminin, fibronectin, collagen type IV and fibrillin[22]. These proteins of the basement membrane promote cell adhesion and cell-cell interaction. Cells in the heart are connected to the ECM through integrins. The integrins bind to intracellular actin filaments through a variety of linker proteins and aid in mechanically coupling intracellular and extracellular structures.

In the past, only the biochemical influence of the ECM had been studied extensively for cardiac cell maturation. With the advent of novel techniques to develop substrates with nanoscale features, now the topographical and mechanical influence of the ECM can be manipulated in conjunction with biochemical cues to mature cardiac cells *in vitro.* The ability to fabricate nanofabricated substrates, mimicking native ECM fibers, will ideally work in tandem with biochemical and mechanical factors to mature stem cell-derived cardiomyocyte phenotype *in vitro*.

1.2.7.1 *Nanotopography*

Kim *et al.*[23] investigated the ultra-structure of the heart and suggested that nanoscale topography is present that is responsible for the structural orientation of native cardiomyocytes. Research findings showed in an *ex vivo* assessment of rat myocardium that the cell alignment was strongly correlated with the alignment of matrix fibers directly

underneath them. This result indicates that a nanoscale orientation and pattern of the ECM could direct the alignment of cardiomyocytes, as suggested by the properties of the ECM (**Figure 1**). This discovery has important implications in the field of cardiac tissue engineering. The results suggest that incorporation of nanotopographical defined substrates into the growth of therapeutic cardiac tissue could increase cardiomyocyte organization and function.

The group engineered nanotopographic surfaces from polyethylene glycol (PEG) hydrogels and seeded neonatal rat ventricular myocytes. Morphological analysis of the cultures on nanopatterned surfaces show clear anisotropy whereas cells cultured on flat substrates showed random cell directionality (**Figure 2**). The study also characterized the effect of nanotopography on electrophysiological properties of engineered myocardium. Electrical stimulation was applied to the center of cell culture substrates from both experimental groups. Action potentials, observed through optical mapping, propagated randomly in all directions for unpatterned substrates while the propagation of action potentials on patterned substrates followed the directionality of the underlying surface topography. The findings provide compelling support for a highly organized structural aspect of cardiac tissue. The size of the nanogrooves, however, will also influence the cell and tissue behavior. Smaller groove widths allow for less cell penetration into the grooves and limit the cell's interaction with the engineering nanotopography[23]. The previous study by Kim *et al.* demonstrated increased conduction velocity on patterns with 800nm groove widths compared to patterns with 400nm groove widths.

1.2.7.2 *ECM Composition*

The composition of ECM present, strongly influences cell adhesion and function. The basement membrane is composed of proteins such as laminin and fibronectin which bind to cells in the heart through integrin receptors. This discovery has led to the wide spread use of these isolated proteins as coating molecules to promote cell adhesion in *in vitro* cultures.

Proteins such as laminin and fibronectin contain an essential amino acid sequence, Arg-Gly-Asp (RGD), which has been shown to serve as a receptor site for integrins during cell adhesion. It is suggested that the RGD sequence is recognized by about half of the 20+ integrins known[2]. Studies have gone to exploit this interaction by synthesizing short peptides with the RGD sequence to immobilize on surfaces for improved cell adhesion[1,25-26]. Recently, efforts have been made to make bifunctional peptides containing the RGD motif, as well as customized domain that selectively binds to a surface of interest.

1.2.7.3 *Mechanical Loading*

Mechanical cues are also largely responsible for tissue development and functional maturation. In addition to topographical and biochemical cues, mechanical cues in the heart also guide cellular organization and modulate contractile function[27-31]. Therefore, many groups have included mechanical stretching to *in vitro* bioreactors as an external influence. Mechanical influences play a strong role in the mechanotransduction process in which mechanical signals are transference to biochemical signals. Stretch stimulation of tissues can benefit many different tissue types including skeletal muscle, ligaments, tendons, and most importantly cardiac muscle[27,32]. The Eschenhagen group were one of

the first groups to show improved force of contraction and tissue organization in response to mechanical stimulus[31]. They have also gone on to change the cardiomyocyte population and *in vitro* shapes to improve blood vessel formation and ease of transplantation.

1.2.7.4 *ECM stiffness*

Although external mechanical stimulus has been studied extensively as a means of modulating cardiac cell behavior, this study attempted to focus more on the inherent mechanical properties of the ECM mimicking substrate. Many previous studies have shown the influence of substrate rigidity on cardiac cell morphology and function[27-32]. However, few studies have investigated the effect of varied substrate rigidity on stem cell-derived cardiomyocytes.

1.2.7.5 *Electrical Stimulation*

The heart also possesses a unique electrical activity which is essential in promoting synchronous contractions. This has prompted many groups to consider the incorporation of electrical stimulus to *in vitro* development of engineered cardiac tissues. Radisic *et al.*[33] investigated the effects of native-like electrical stimulation on the production of functional myocardium *in vitro*. The goal of this study was to mimic the physiological electrical environment of the native heart during culturing of cardiomyocytes on scaffolds. The cell constructs were placed into a glass chamber containing 2 ¼ inch diameter carbon rods. Silicon spacers were used to separate wells. The chamber received electrical stimulation by a cardiac stimulator connected to platinum wires that were then connected to the

carbon rods within the chamber. A constant pulsatile electrical stimulation was applied for 5 days to mimic physiological ranges of electrical activity (square wave, 2ms, 5 V/cm, 1Hz). Simultaneous culture of a cell construct without electric stimulation was also performed for comparison. The results of this study indicated that the presence of electrical stimulation resulted in a dramatic increase in the contractile properties of the cell constructs. The study displayed that the strength of contraction was 7 times higher for the cell construct that had received electrical stimulation than non-stimulated tissue constructs, after 8 days of culture. The presence of electrical stimulation also resulted in increased levels of Myosin Heavy Chain, Cx-43, creatine kinase-MM, and cardiac Tn-I, among other factors. Another notable improvement of the myocardium subjected to electrical stimulation was the orientation and coupling of cells. The cells had increased their alignment, elongation, and central positioning of nuclei. These findings present promising data that support the improved function of cardiomyocytes subjected to electrical stimulation.

Further studies have gone on to combine electrical signals with native-like topography to promote cardiomyocyte maturation[54]. The study demonstrated cell elongation and alignment along microgrooves in the direction of the external electrical field while also showing confined gap junction formation to cell-cell end junctions. Although studies have focused on the incorporation of electrical signals into cardiomyocyte cultures, either individually or in combination with other cues, much of the electrical stimulus based studies have focused on rat models.

1.3 *Summary*

In summary, efforts to improve cardiac repair, drug screening, and disease modeling have led researchers to hPSC-CMs. However, the immature state of hPSC-CMs have limited the ability of groups to improve the above mentioned areas. Consequently, focus has shifted to establishing *in vitro* environments which promoted hPSC-CM maturation towards adult cardiomyocyte phenotypes. In order to mature cardiomyocytes *in vitro* researchers have begun trying to mimic the native environment of the heart *in vitro*. Because of the extreme complexity of the myocardial environment it has proved difficult to optimally develop such environments *in vitro*. Regardless, ongoing efforts look to establish synergistic platforms that are able to effectively integrate multiple components of the native environment to promote hPSC-CM maturation.

1.4 *Thesis Outline*

In this thesis we intend to use the biophysical properties of the native heart to develop an environment in which we can mature hPSC-CMs. We hypothesize that the degree to which the native environment can be mimicked correlates directly to the ability of hPSC-CMs to mature towards an adult cardiomyocyte phenotype. We will present the combination of multiple native heart characteristics meant to provide a platform for structural and functional maturation of cardiomyocytes.

In chapter 2, we present previous work in which nanoscale topography was combined with native like electrical stimulation to promote maturation of neonatal rat ventricular myocytes. It was proposed that the synergistic effect of topographical and

electrical stimulation would elicit a higher degree of maturation compared to constructs that were not stimulated and seeded on unpatterned substrates. We intended to evaluate cardiomyocyte maturation through overall morphology, sarcomere length, cardiac gene expression, and gap junction protein expression.

In chapter 3, we propose the development of a combinatorial platform that can be used to mature hPSC-CMs. First, we intended to develop a substrate with differential nanoscale topographic dimensions as well as an unpatterned control to highlight the effect of topography on hPSC-CM maturation. Next, we intend to develop a biofunctionalized peptide that contains one domain which can selectively bind to our substrate of choice and another domain that is meant to interact with integrin proteins present in hPSC-CM. Finally, we propose combining the differential topographic platform with the custom synthesized bifunctional peptide to determine the platform viability with hPSC-CM culture.

In chapter 4, we propose the use of the combinatorial platform for structural maturation of hPSC-CMs. We intended to investigate the combinatorial benefit of the platform developed in chapter 3 on both hESC-CMs and hiPSC-CMs. We propose a 3 week culture of single cell hPSC-CMs followed by analysis of structural maturation. We intend to determine the degree of structural maturation through analysis of cell area, perimeter, circularity, alignment, and sarcomere length. In chapter 5, we present our conclusions of the studies discussed in the thesis and briefly present on going and future work.

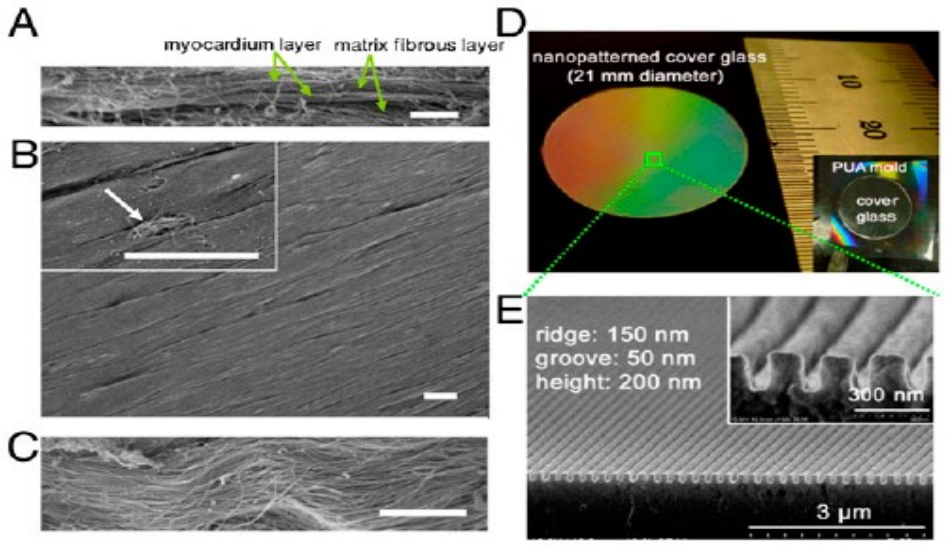

Figure 1. A-C: Ex vivo assessment of rat myocardium where A is a side view, B is a top view, and C is a magnified view. D: ANFS on glass cover slip. E: Cross section of ANFS[23].

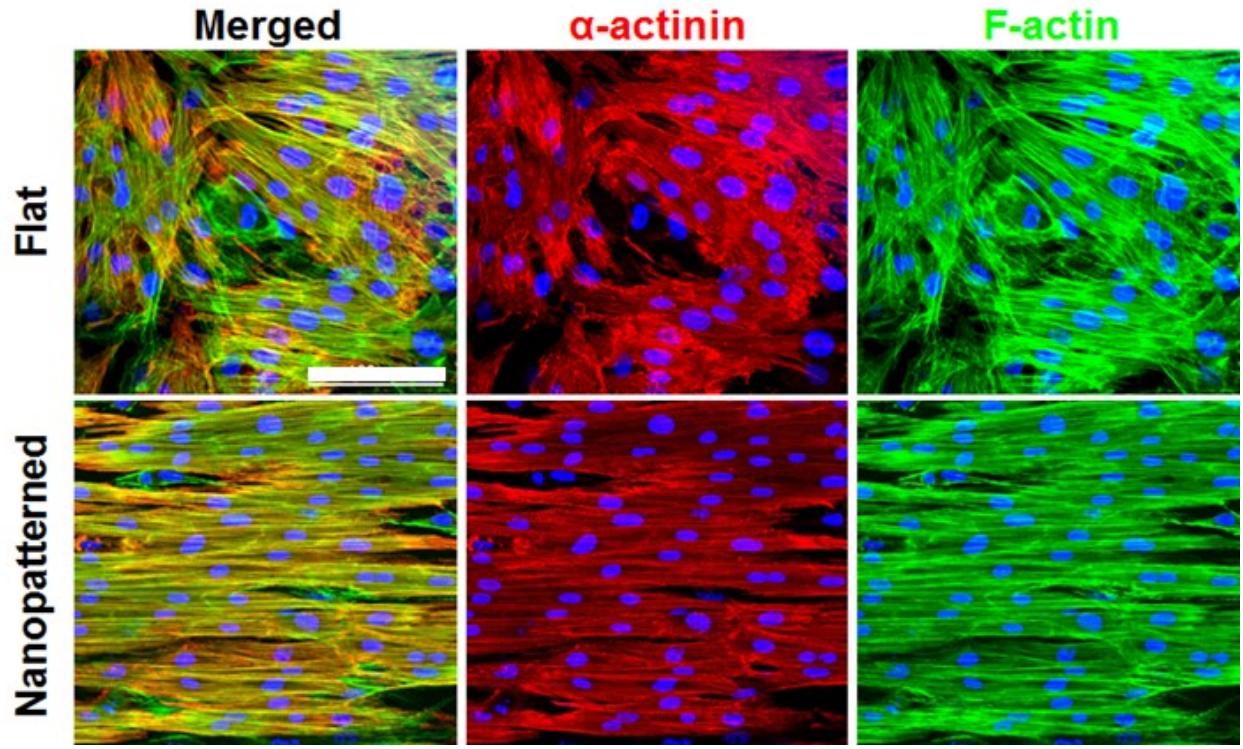

Figure 2. NRVM immunostained images on flat and 800nm (1:1) PEG substrates. Figure includes merged image, alpha-actinin image (red), and F-actin image (green). Cells on nanopatterns exhibit high degree of anisotropy compared to flat substrates (Day 7 of culture). Scale bar: 100μm.

CHAPTER 2: NANOTOPOGRAPHIC AND ELECTRICAL STIMULATION OF NEONATAL RAT VENTRICULAR MYOCYTES

2.1 *Introduction*

In a previous study in our lab, the concept of applying electrical stimulation to cardiac constructs was used in conjunction with nanotopographically defined substrates to investigate maturation of neonatal rat ventricular myocytes. The goal of this project was to use native characteristics of the heart to develop an *in vitro* environment suitable for NRVM maturation.

2.2 *Materials and Methods*

Fabrication of Nanopatterned Substrates

All NOA (Norland Optical Adhesive) substrate fabrication was accomplished by UV-assisted capillary force lithography. Prefabricated silicon masters (1st generation master) were used as the starting step in the fabrication of nanopatterned substrates. 40μL of PUA (poly(urethane acrylate)) 301 (19.8 MPa) was dropped dispensed on clean silicon master surface (100% ethanol or xylene and dry under O_2/N_2 gas). A sheet of 4cm x 4cm transparent polyester (PET) film was placed over the dispensed PUA. The silicon master, prepolymer, and PET were placed approximately 10cm below a 20 Watt (115V) UV light (λ = 365nm) for 50 seconds. The intensity of the light was 100mW/cm^2 at the surface of the substrate. After curing, the PET film was slowly removed with forceps. PUA should attach to the PET film with a negative of the silicon master nanopattern. The PUA/PET nanopatterns were then cured under UV for at least 12 hours prior to use. The next step in the process involves using the 2nd generation master to pattern NOA substrates on

glass slides that would be used for biological experiments. Glass slides were cleaned for 20min in isopropyl alcohol, ozone treated for 10 min, and coated with glass primer to increase adhesion of the NOA polymer to the surface. 10μl NOA polymer was drop dispensed on the pretreated glass slide and the nanopatterned master was placed face down on the polymer/glass surface. The glass slides (plus master) were UV cured for 50 seconds followed by peeling off the master from the glass surface (**Figure 3**).

NRVM Isolation

The cell source used for the stimulation experiments was neonatal rat ventricular myocytes (NRVM's) acquired through primary isolations of rat pups. The procedure involved sacrifice of neonatal rats (decapitation) followed by extraction of the hearts. The hearts were placed into a cooled Ads buffer where the aorta was subsequently detached from the ventricle. After removal of aortic components, ventricles were minced into smaller fragments; smaller fragments increase efficiency of cell extraction. The next part of the procedure involved incubation for 30 minutes of minced ventricles in prepared digest solution (Ads buffer, w/ collagenase II, w/ protease XIV). Supernatant was then collected, cells were spun down using centrifuge, supernatant was then aspirated off, and cell pellet was re-suspended in plating media. These digest steps were repeated 5 times to ensure collection of maximum amount of NRVM's. Optimization for this procedure required alteration of several steps in the process. As the process was adapted from the Regnier lab, pups were sacrificed at an age range between 24 and 72 hours. It was found that the age of the rat had a strong influence on the viability of isolated cells. The pH of the digest solution was also a key factor that was altered during the digestion process.

Cell Culture

NRVM's were seeded at a density of 1.25 million/cm^2 into 6 well MatTek dishes. Culture was maintained for 7 days with daily media change. Media used consisted of the following: DMEM (high-glucose, -sodium pyruvate), HEPES, M199, Horse Serum, Fetal Bovine Serum, and Pen-Strep. Ara-C (10 μm) was used to eliminate proliferating cells (pure cardiomyocyte culture).

Electrical Stimulation

Stimulation was performed using commercially available 6 well cartridges from IonOptix. Cells were subjected to stimulation starting 24 hours after seeding; stimulation was maintained to end of experiment. Stimulation parameters used were: Amplitude (3V/cm), Frequency (3Hz), Duration (2ms), Wave Type (square).

Immunostaining

Cells were fixed at the end of 7 days of culture with 4% paraformaldehyde (Affymetrix). Cells were then rinsed twice with PBS and permeabilized with .1% Triton-X-100 in PBS for twice for 5 minutes. Samples were then blocked with 1% bovine serum albumin (in PBS) for 40-60 minutes at room temperature. Primary antibodies were then diluted in 5% BSA: alpha-actinin 1:1000 (sigma Aldrich incubated for 1 hour at room temperature. Secondary antibodies were diluted in 5% BSA to match dilution of primary antibody dilution: Alexa Fluor-594 was used for alpha actin and conjugated Alexa-Fluor488/-Phalloidin was used for cytoskeleton staining. Samples were incubated at 37°C with

secondary antibodies for 1 hr. Samples were then washed with PBS and prepared with VectaShield + DAPI and stored in 4°C until confocal imaging.

Western Blot Analysis

Cx-43 protein expression was examined using a standard western blot protocol. First, cells are lysed and broken down to extract protein contents. The proteins are separated by gel electrophoresis, which separates Cx-43 based on molecular weight. Next, the separated protein is transferred from the gel to a nitrocellulose membrane by electroblotting. The surface is than blocked with 5% BSA to prevent non-specific binding. The following step involves a wash with the Cx-43 primary antibody followed by Alexa Fluor-488 secondary antibody. The samples are then mounted and prepared for detection.

quantitative-PCR analysis

Cardiac gene expression was examined using q-PCR follow the standard Qiagen kit. Steps involve tissue/cell lysis and cDNA extraction. The cDNA is transcribed to associated mRNA and loaded in a 96-well dish. The 96-well dish is then subjected to a thermocycle process which sequentially amplifies the gene signal for detection.

2.3 *Results/Discussion*

The results obtained from our previous study were promising, but also left several questions to answer. Many of the qualitative assessments associated with the project

yielded promising findings, while many of the quantitative results were contradictory. In brief, one must trust the quantitative over qualitative results.

Morphological analysis of the experimental conditions showed a positive effect of electrical stimulation and underlying surface topography. F-actin (cytoskeleton) stains showed tissue more representative of the native heart for electrically stimulated (nanotopographic) constructs; they were elongated and thick (**Figure 4**). One limitation of this section was the inability to quantitatively measure cell morphology. Analysis of bright field images was difficult because monolayer formation prevented distinction of cell borders. Efforts to use live cell dyes and cell border stains were unsuccessful.

Immunostaining eventually yielded very attractive visual results, as mentioned above. Cellular alignment, as demonstrated by F-actin staining, followed predicted trends while alpha-actinin showed the clear presence of a primary cardiomyocyte population. Connexin-43 staining for localization purposes was much more difficult to achieve. One possible reason may be due to the thickness of the tissue constructs with prolonged culture and delayed stimulation. The success of alpha-actinin staining enabled quantitative analysis of sarcomere lengths within each condition population. Our results displayed the clear synergistic effect of electrical stimulation and surface topography on sarcomere length (**Figure 5**).

Western blot analysis and q-PCR were two of the data sets that were not able to yield conclusive results. Although connexin-43 expression appeared to be upregulated in electrically stimulated nanopatterned constructs, it was not statistically significant (**Figure 6**). Q-PCR analysis was used as a key determinant of maturity. Indications of maturity of would be increases in alpha-MHC/beta-MHC and fs-Tnni/ss-Tnni ratios. The

roles of ANP and BNP remain in debate as to their role in maturity; as they may indicate pathological hypertrophy. The lack of conclusive results from these two assays indicates the possibility that electrical stimulation 24 hours after primary cell isolation may suppress gene expression and establishment of gap-junctions (**Figure 7**).

2.4 *Summary*

One of the major limitations associated with this previous study was the inconsistent cell attachment across experimental trials. Although some inconclusive results in maturity assays are most likely attributed to premature stimulation, cell attachment also plays an integral role. Without a confluent monolayer, the entire population of cells cannot communicate effectively. This can slow down maturity of the construct on many hierarchical levels.

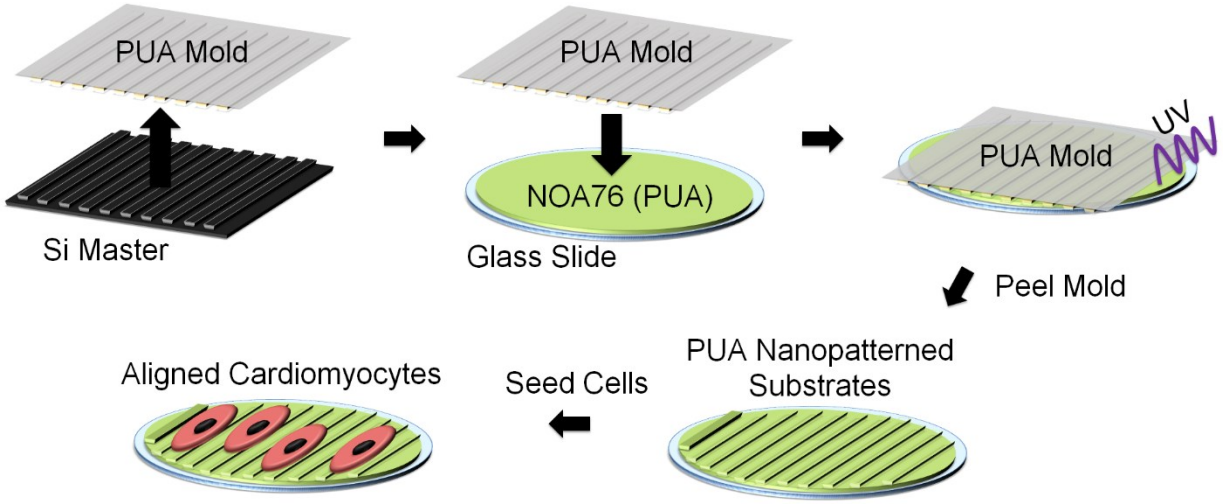

Figure 3. Schematic representing the UV-assisted capillary force lithography fabrication process of nanotopographically defined substrates.

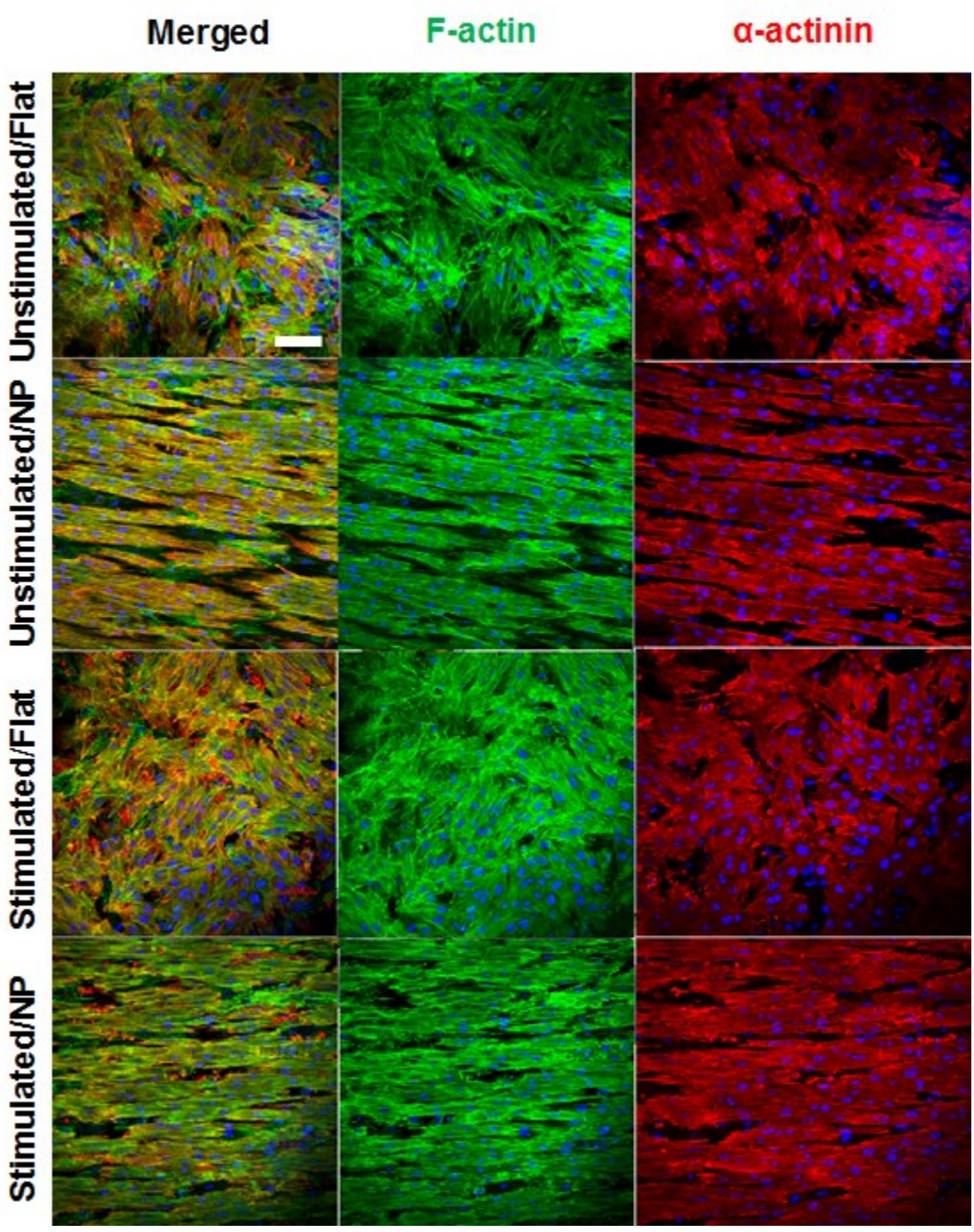

Figure 4. NRVM immunostained images. From top to bottom: Unstimulated Flat, Unstimulated NP, Stimulated Flat, and Stimulated NP. Scale bar: 50 μm.

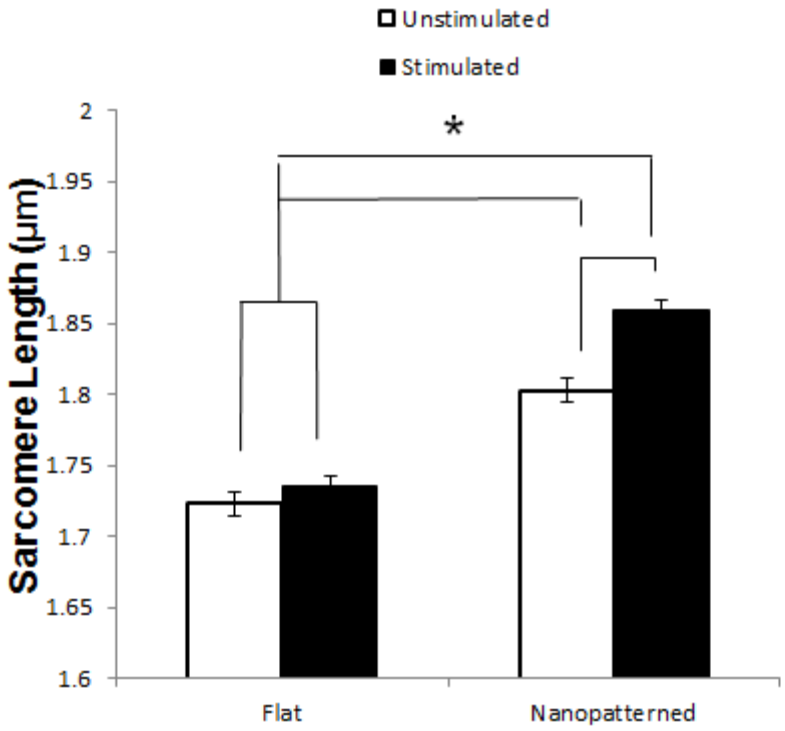

Figure 5. Sarcomere length of each of four conditions. N = 45-50 cells per condition. SEM for each condition was found to be approximately .017 um. P values for unpaired t tests: ES/US Nano = .0201, US Flat/Nano = .0039, ES Flat/Nano < .0001.

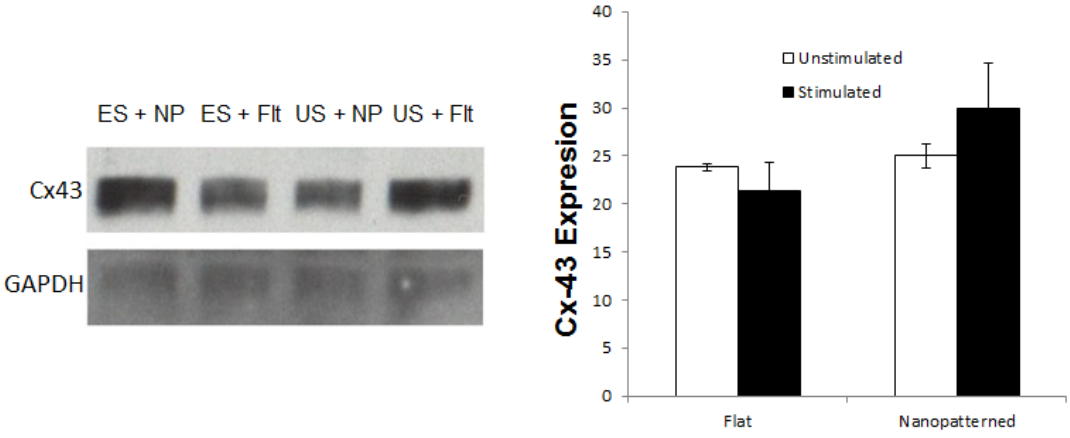

Figure 6. Western blot trial, Cx-43 expression, with standard deviations included. No significant differences observed across conditions.

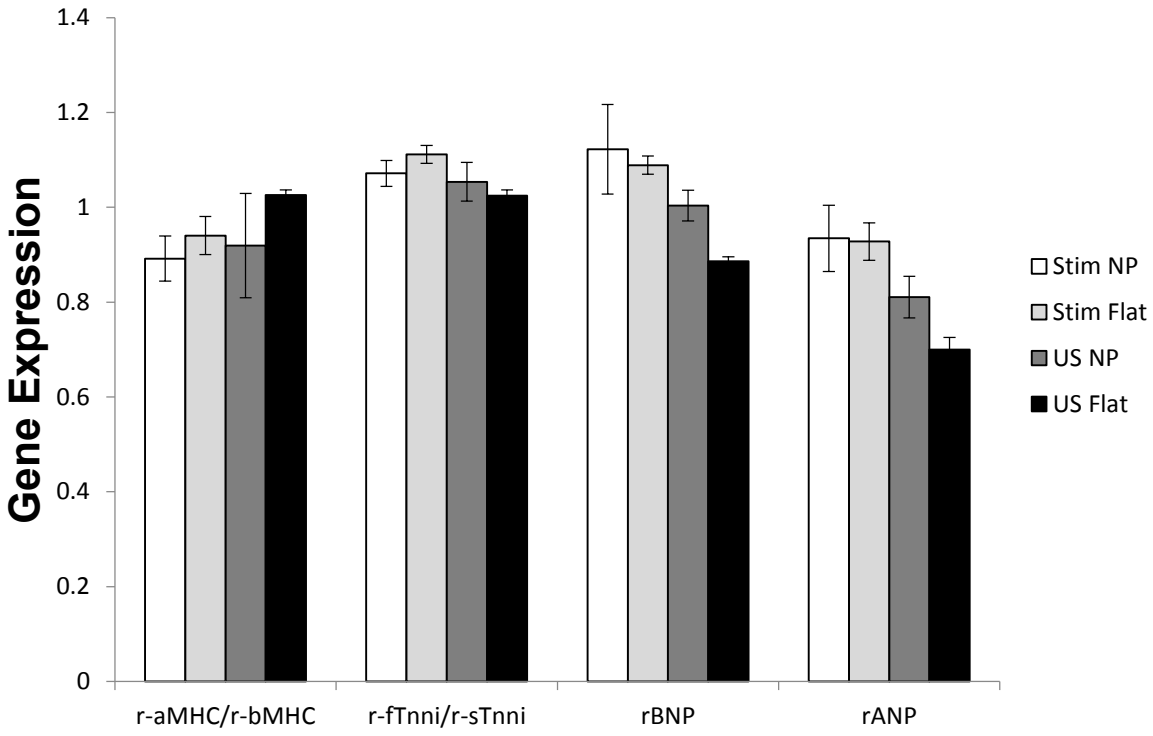

Figure 7. Represents q-PCR assay results for four conditions: r-aMHC/r-bMHC ratio, r-fTnni/r-sTnni ratio, rBNP, rANP. All normalized to GAPDH control. SEM for samples varied, max observed for stim NP rBNP at .031. Statistically significant results not observed.

CHAPTER 3: ENGINEERING A MATRIX PLATFORM FOR DEVELOPMENT OF HPSC-CMS

3.1 *Introduction*

Cardiac tissue engineers have investigated numerous techniques of incorporate single or multiple characteristics of the native heart environment into design of *in vitro* engineered tissues. As mentioned, the complex structure of the heart is organized on multiple scales and is present to help direct the collective movement of action potentials along tissue, providing strong synchronous contractions. Tissue alignment can be seen on all levels, from the 3-dimensional ultra-structure down to the micron scale sarcomeres. Although anisotropic cardiac tissue *in vivo* can be attributed in part to multiple scale interactions of organized fiber components, the influence of the underlying extracellular matrix plays a critical role. The underlying topography of the ECM makes up the immediate structural guidance cue for cardiomyocytes. Other properties of the ECM such as the mechanical integrity and embedded biochemical cues play a significant role in cardiac cell phenotype.

In our study we wanted to focus on how these ECM characteristics could be manipulated to mature stem cell-derived cardiomyocyte phenotype for applications such directed therapy, cardiac drug screen, and heart disease modeling. However, first we want to ensure that we could develop a combinatorial platform that integrates key components of the native ECM.

3.2 *Methods and Materials*

Fabrication of Nanopatterned Substrates

All NOA (Norland Optical Adhesive) substrate fabrication was accomplished by UV-assisted capillary force lithography. Prefabricated silicon masters (1st generation master) were used as the starting step in the fabrication of nanopatterned substrates. 40μL of PUA (poly(urethane acrylate)) 301 (19.8 MPa) was dropped dispensed on clean silicon master surface (100% ethanol or xylene and dry under O_2/N_2 gas). A sheet of 4cm x 4cm transparent polyester (PET) film was placed over the dispensed PUA. The silicon master, prepolymer, and PET were placed approximately 10cm below a 20 Watt (115V) UV light (λ = 365nm) for 50 seconds. The intensity of the light was 100mW/cm^2 at the surface of the substrate. After curing, the PET film was slowly removed with forceps. PUA should attach to the PET film with a negative of the silicon master nanopattern. The PUA/PET nanopatterns were then cured under UV for at least 12 hours prior to use. The next step in the process involves using the 2nd generation master to pattern NOA substrates on glass slides that would be used for biological experiments. Glass slides were cleaned for 20min in isopropyl alcohol, ozone treated for 10 min, and coated with glass primer to increase adhesion of the NOA polymer to the surface. 10μl NOA polymer was drop dispensed on the pretreated glass slide and the nanopatterned master was placed face down on the polymer/glass surface. The glass slides (plus master) were UV cured for 50 seconds followed by peeling off the master from the glass surface (**Figure 3**). Protocol deviations for full patterns versus 4x4 island patterns only occurred in the original master fabrication. Island pattern masters were obtained from prefabricated 4x4 silicon masters (350nm – 2000nm) (**Figure 8)**.

PUABP-RGD Synthesis/Characterization

The peptide was chosen after screening a library of 15 peptides. The screening assay took PUABP candidates conjugated to biotin and coated a PUA surface. A streptavidin-Alexa conjugate was added to determine the degree of immobilization of the PUABP candidates to the PUA surface. The biotin section of immobilized peptides would conjugate with streptavidin and emit fluorescence **(Figure 9)**. The PUA binding peptide + RGD (PUABP1-RGD (MW 2155.4), PUABP2-RGD (MW 2011.3)) was synthesized by solid-state synthesis using a CSBioe 336s automated peptide synthesizer on Wang resin via Fmoc chemistry and HBTU activation[1]. The crude PUABP-RGD peptide was purified by reverse phase high performance liquid chromatography. The purified PUABP2-RGD was verified by mass spectroscopy using a MALDI-TOF mass spectrometer. Surface coverage of PUABP-RGD was accomplished similar to the screening process. PUABP candidates conjugated to biotin were coated on the PUA surface. They were incubated with streptavidin-Alexa and fluorescence microscopy was used to image the surface and determine the amount of coverage through biotin-SA-Alexa conjugation **(Figure 10)**.

hESC-CM Differentiation

RUES2 cardiomyocyte differentiation was accomplished using an established protocol. Replated human embryonic stem cells were induced with RPMI-B27 medium plus supplemental activin A (100ng/mL) at a volume of 1mL per well of a 24-well plate. After 24 hours the activin A containing medium was replaced with 1 mL of RPMI-B27 with supplemental BMP-4 and cultured for 4 days without medium change. At day 5, the BMP-4 containing medium was replaced with 1mL of RPMI-B27 medium. After day 5 cells are fed with RPMI-B27 medium every other day and monitored for spontaneous beating

activity which reaches is peak around day 14. The differentiated cardiomyocytes are then fed until replating for *in vitro* experiments between days 18-20 **(Figure 11)**.

hiPSC-CM Differentiation

IMR90 cardiomyocyte differentiation was accomplished using a protocol established by James Thomson[13]. The protocol is similar to that of the directed differentiation of the RUES2 cardio cell line. In addition to serial application of activin A and BMP-4, cultures were supplemented with Wnt agonist CHIR 99021 in early stages and followed with Wnt antagonist Xav 939. The differentiated cardiomyocytes are then fed until replating for *in vitro* experiments between days 18-20 **(Figure 11)**.

Cell Culture

Human embryonic stem cell-derived cardiomyocytes (RUES2) and human induced pluripotent stem cell-derived cardiomyocytes (IMR90) were used for this study. In single cell experiments, cells were seeded at a density of 15,000 cells per cm^2. Culture medium (RPMI +B27 + Insulin) was changed every other day throughout the length of the experiment (2mL). Prior to cell seeding, substrates were coated with 750uL fibronectin (50ug/ml), PUABP1-RGD (100uM), or PUABP2-RGD (100uM) and incubated overnight at 37°C.

3.3 *Results/Discussion*

We present the development of an array of nanopattern dimensions (350nm – 2000nm) using a 4x4 island platform. This platform makes it possible to screen 16 nanopatterned dimensions as well as a flat control in a single well **(Figure 8)**. Scanning electron

microscopy imaging verified pattern dimensions (4 representative images of island corners shown). In combination we demonstrate the incorporation of specialized ECM composition. Building on the information presented by previous studies we have developed a bifunctional peptide containing the RGD sequence as well as a customized domain that selectively binds to our PUA substrates, named PUA binding peptide-RGD (PUABP-RGD). The peptide was chosen after screening a library of 15 peptides. The screening assay took PUABP candidates conjugated to biotin and coated a PUA surface. A streptavidin-Alexa conjugate was added to determine the degree of immobilization of the PUABP candidates to the PUA surface. The biotin section of immobilized peptides would conjugate with streptavidin and emit fluorescence. The two candidates with the highest fluorescence emission were chosen moving forward.

It is predicted that the customized PUA domain of the bifunctionalized peptide will increase uniformity of attachment to the substrate and thus promote increased cell attachment and long term maintenance of cell monolayers. Both PUABP candidates were again bound to biotin and incubated on PUA surfaces with SA-Alexa. Florescence microscopy was then used to image the surface of the bound peptides compared to controls. The PUABP-biotin samples displayed uniform fluorescence across the surface of the images while controls (bare surface, SA-Alexa without PUABP-biotin) displayed no fluorescence **(Figure 10)**. Quantitative average fluorescence values were also obtained to determine the about binding at distinct areas. Interestingly, the average fluorescence readings were increased for PUABP2-biotin compared to PUABP1-biotin, while both were much higher than the control.

Prior to the incorporation of the PUABP-RGD into hPSC-CM cultures, C2C12 adhesion was investigated in response to the bifunctional peptide incorporation. **Figure 12** displays the influence of PUABP2-RGD on cell adhesion with C2C12 cells and is compared to adhesion on substrates without peptide coating. Both the glass control condition and Flat PUA without peptide coating appear to have no significant cell attachment; most visible cells in field of view are rounded up and out of focus which indicate the absence of attachment to the substrate. Nanopatterned PUA without peptide coating shows improved cell attachment and alignment compared to flat and glass controls, but also maintain a large percentage of unattached cells. PUABP-RGD incorporation displays dramatic improvement in C2C12 adhesion compared to conditions without. The figure also elucidates the cell morphology differences between flat and patterns conditions as cells on the patterned substrate become elongated and aligned.

Encouraging results from preliminary adhesion experiments with PUABP-RGD and C2C12's led to the concept of incorporating the peptide in hPSC-CM cultures. A cell adhesion studied was performed to determine the viability of PUABP-RGD in human stem cell-derived cardiomyocyte studies. Two hPSC-CM cell lines were investigated for cell adhesion: RUES2 cardios (embryonic derived) and IMR90 cardios (somatic cell derived, reprogrammed). Cells were seeded on 4 x 4 island patterned substrates (PUA, 6.7 MPa), at 15,000 cells/cm^2, that had been coated with fibronectin (50ug/ml), PUABP1-RGD (100uM), or PUABP2-RGD (100uM) (**Figures 13-15**).

At 24 hours attached cells were counted for each condition (**Figures 16, 17**). For both cell lines there were no significant differences in cell attachment between pattern dimensions and ECM coating. It was expected that the ability of the bifunctional peptide

to selectively adhere to the PUA surface would provide more uniform coating then nonspecific protein adsorption of fibronectin. While this may in fact be true, the density at which cells were seeded, for single cell evaluation, showed comparable results for cell adhesions between conditions. This result is positive as it provides a more specific alternative to isolated ECM proteins for engineering cardiac tissue *in vitro*. The potential of improved uniformity in ECM coating may provide a benefit for monolayer experiments. It is also important to note that there was not a significant difference in cell attachment between nanogroove widths. While it is expected that the change in dimensions will elicit different cell responses over time, the initial attachment similarities suggests uniform ECM coating and cell dispersion. It is important to note that although PUABP1-RGD showed positive results in cell attachment, PUABP2-RGD was used as a comparison to fibronectin for cell maturity studies as extensive characterization of PUABP1-RGD has yet to be accomplished.

3.4 *Summary*

In summary, we demonstrate the development of a platform which combines 16 nanoscale pattern dimensions (plus flat controls) and the ability to incorporate different ECM compositions. Part of the development process involved synthesis of a bifunctionalized peptide meant to serve as an ECM alternative to commonly used proteins such as fibronectin. We demonstrate successful synthesis of two strong candidates (PUABP1-RGD/PUABP2-RGD) to be used in cell experiments. The ability of the customized PUA domain of the peptide to bind to our PUA substrates was evaluated and through biotin-SA-Alexa conjugation experiments and showed a high affinity for the surface as well as uniform surface coverage.

Next we wanted to investigate the ability of cells to adhere to substrates coated with the customized peptide. Initial trials with C2C12 cells shown promoted cell adhesion on surfaces coated with the peptide compared to surfaces without the peptide. We then accomplished more extensive studies of hPSC-CM attachment on the engineered 4x4 island platform coated with either of the two PUABP-RGD peptides and fibronectin. Quantitative analysis of cell attachment 24 hours post seeding showed that the cell attachment was similar across all dimensions and ECM coating molecule suggesting the ability of PUABP-RGD to function as an alternative to more commonly used proteins such as fibronectin. These results are promising when considering monolayer studies. It is expected that the uniformity of peptide attachment to the PUA substrates will improve hPSC-CM monolayer formation and long term maintenance.

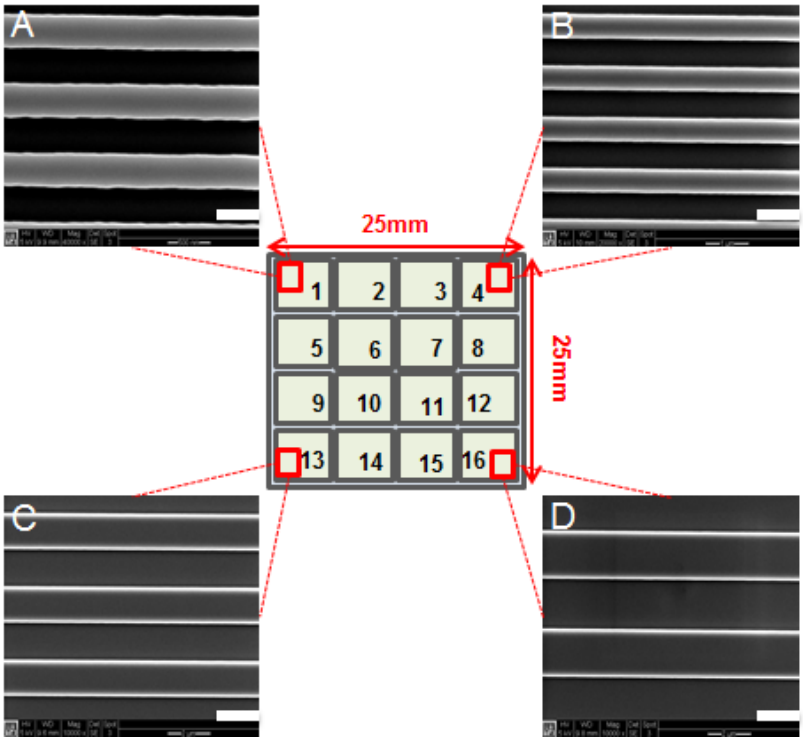

1	w : 350 P : 700	9	w : 900 P : 1800
2	w : 400 P : 800	10	w : 1000 P : 2000
3	w : 450 P : 900	11	w : 1200 P : 2400
4	w : 500 P : 1000	12	w : 1250 P : 2500
5	w : 600 P : 1200	13	w : 1500 P : 3000
6	w : 700 P : 1400	14	w : 1600 P : 3200
7	w : 750 P : 1500	15	w : 1800 P : 3600
8	w : 800 P : 1600	16	w : 2000 P : 4000

Figure 8. Schematic of 4x4 island nanopattern platform. SEM images demonstrate surface dimensions of platform corners. Table to right corresponds to pattern dimensions for each square in figure to left. Scale Bar: (A) 500nm (B) 1μm (C) 2μm (D) 2μm.

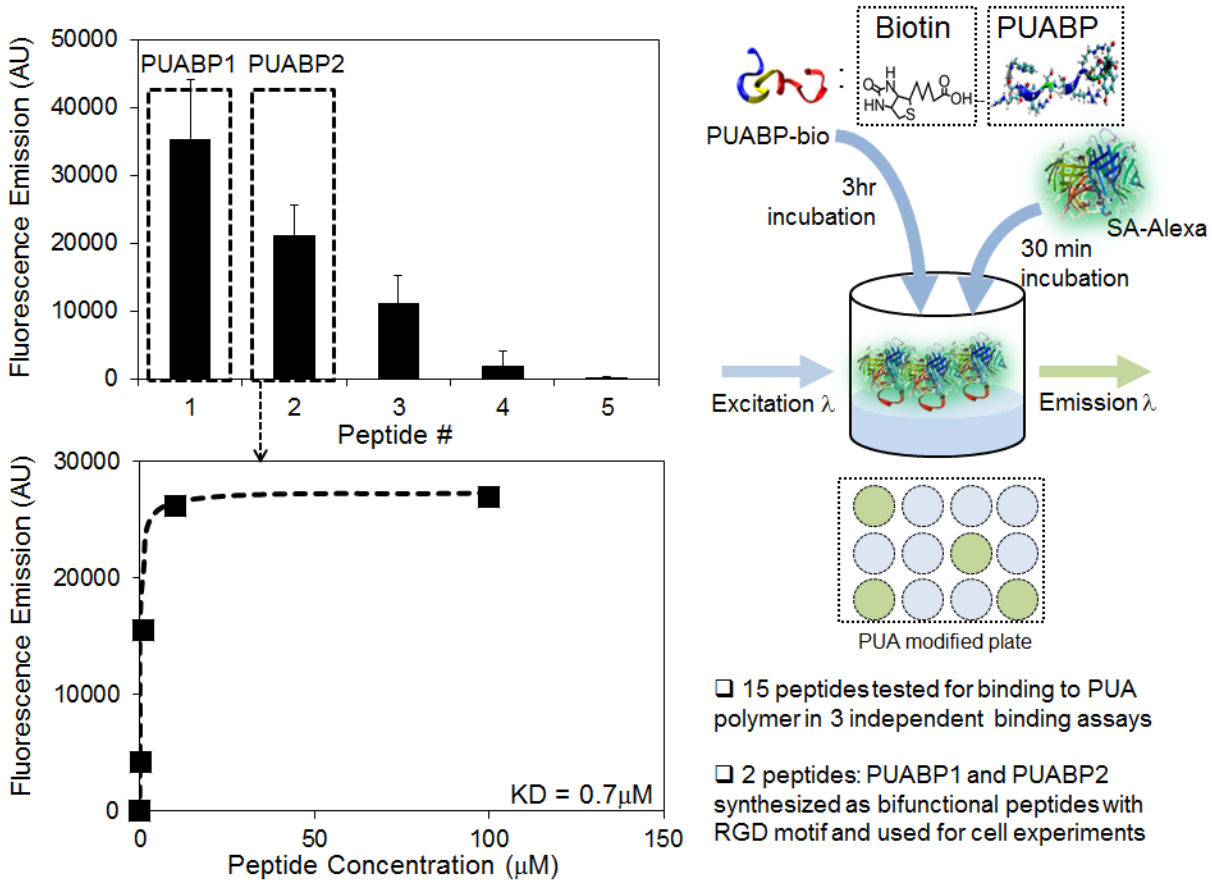

Figure 9. PUABP2-RGD characterization. PUABP-biotin incubated with SA-Alexa to determine degree of affinity for substrate surface based on fluorescence emission with biotin-SA conjugation. Concentration binding curve calculated for PUABP2-RGD, saturation at 100µ M. Kd= .7.

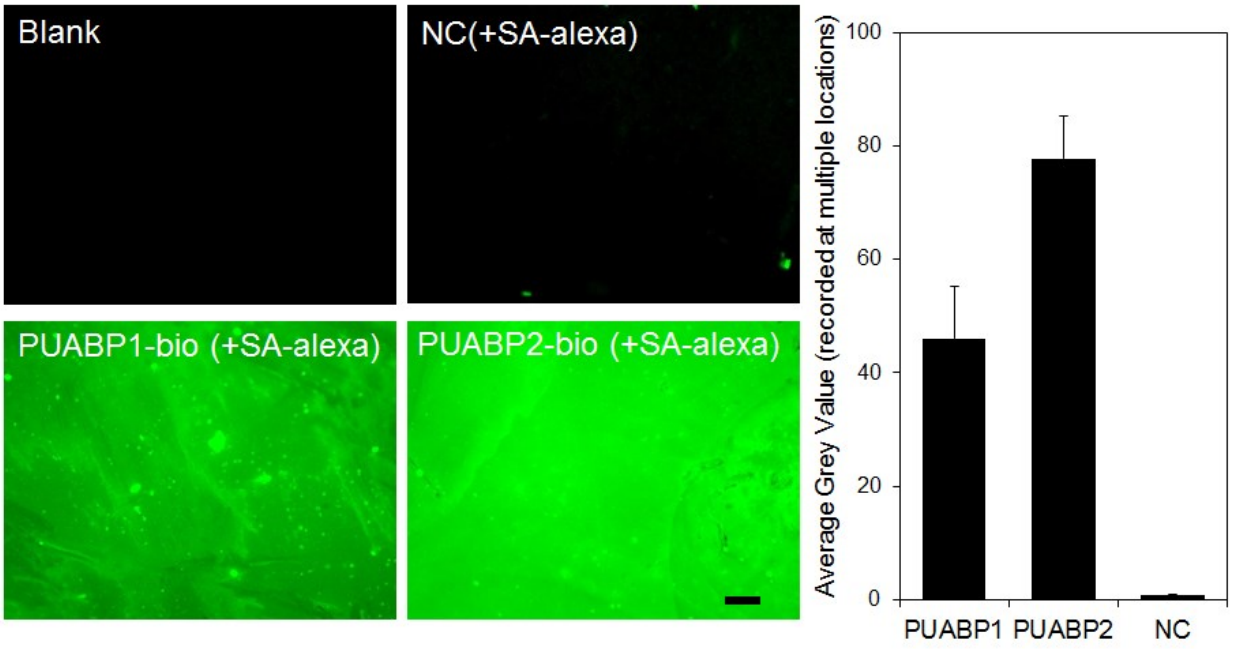

Figure 10. PUABP-RGD surface coverage characterization. PUABP-biotin incubated with SA-Alexa on PUA substrates. Fluorescent Microscopy used to determine surface binding density compared to blank surface and SA-Alexa without PUABP-biotin. Average fluorescent intensity also measured at multiple locations on substrates. PUABP2-biotin displayed similar surface coverage compared to PUABP1-biotin, but a higher average fluorescent intensity. Scale bar: 20μm.

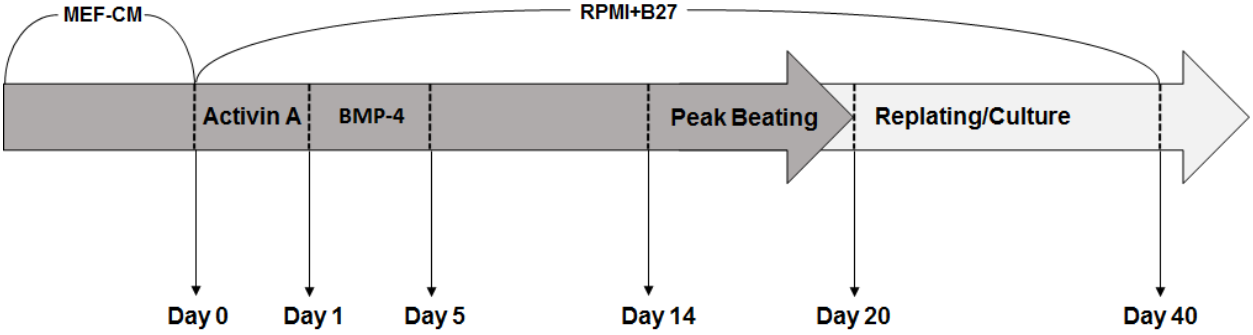

Figure 11. Schematic of stem cell-derived cardiomyocyte differentiation process. At Day 0, undifferentiated cells are induced with activin A, followed by BMP-4 at Day 1-5. Cells are cultured until day 18-20 prior to replating. Prior to Day 0 undifferentiated cells were cultured in mouse embryonic fibroblast-conditioned medium. After Day 0 media was changed to RPMI + B27 supplement.

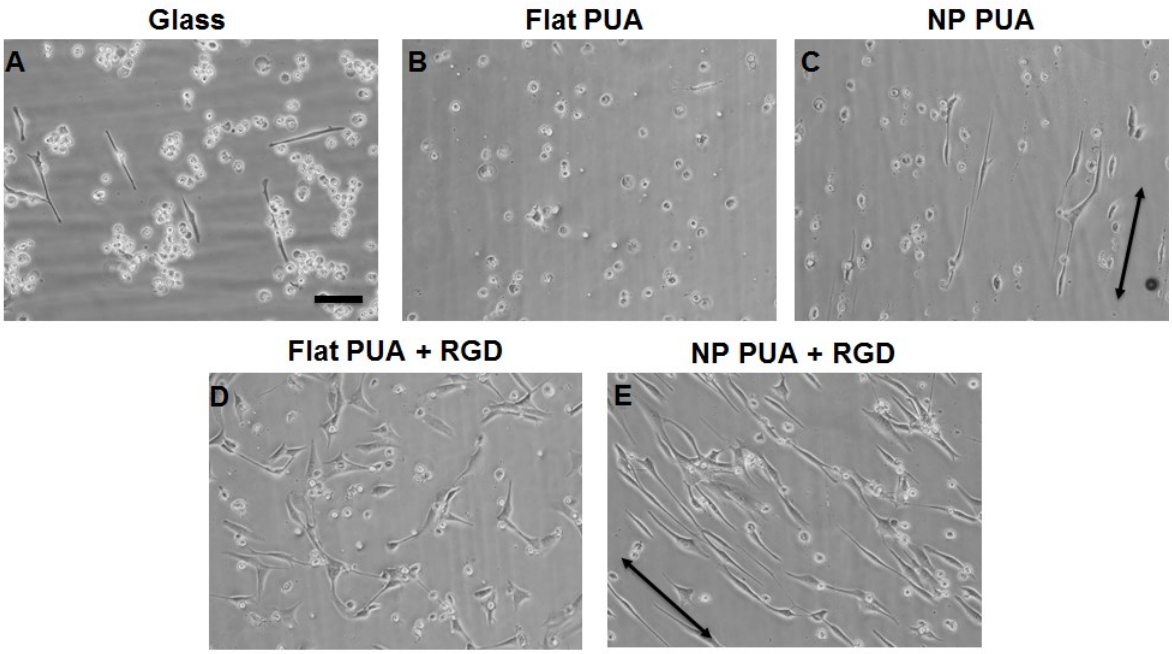

Figure 12. C2C12 cell attachment 24 hours after seeding. (A) Glass control (no adhesion), (B) Unpatterned PUA scaffold without RGD (low adhesion), and (C) Patterned PUA scaffold without RGD (low adhesion). (D) Unpatterned PUA scaffold with RGD (high adhesion) and (E) Nanopatterned PUA scaffold with RGD (high adhesion). Scale bar: 50μm.

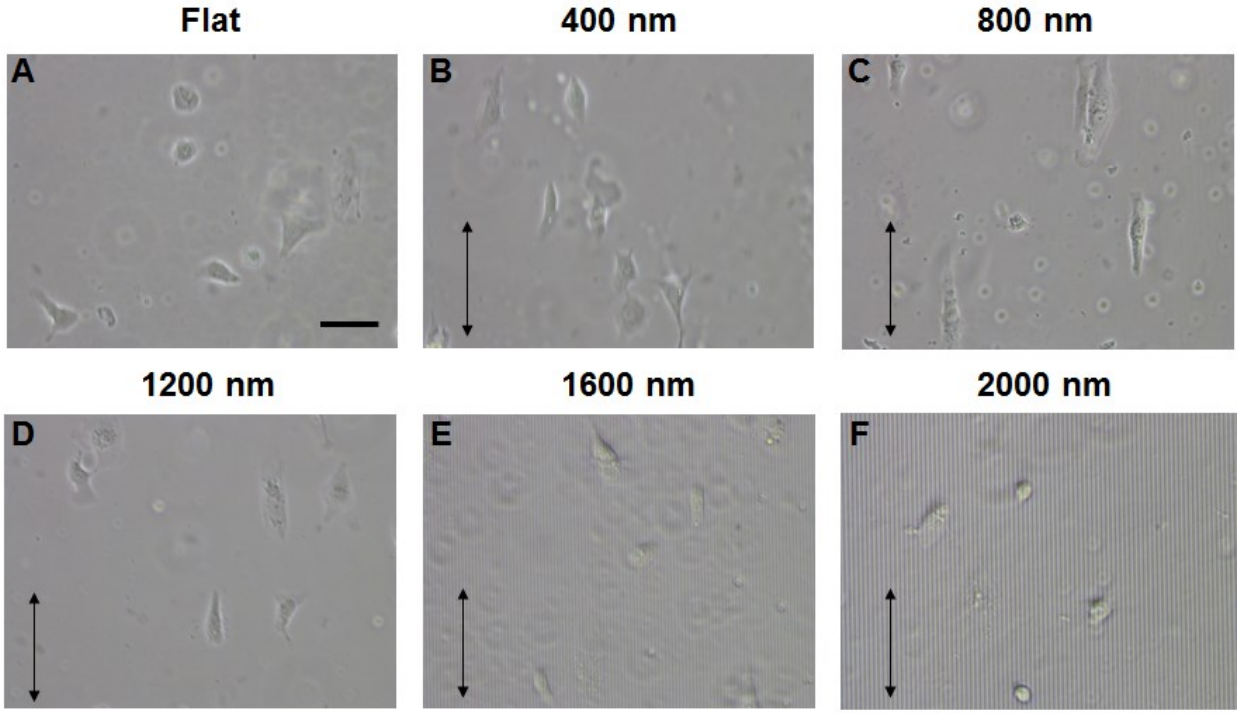

Figure 13. IMR90 cardio adhesion of fibronectin (50μg/ml) coated 4x4 island patterns 24 hours post replating. Conditions include following nanogroove widths (A) flat, (B) 400nm, (C) 800nm, (D) 1200nm, (E) 1600nm, and (F) 2000nm. No significant differences in cell adhesion among pattern dimensions observed. Scale bar: 50μm.

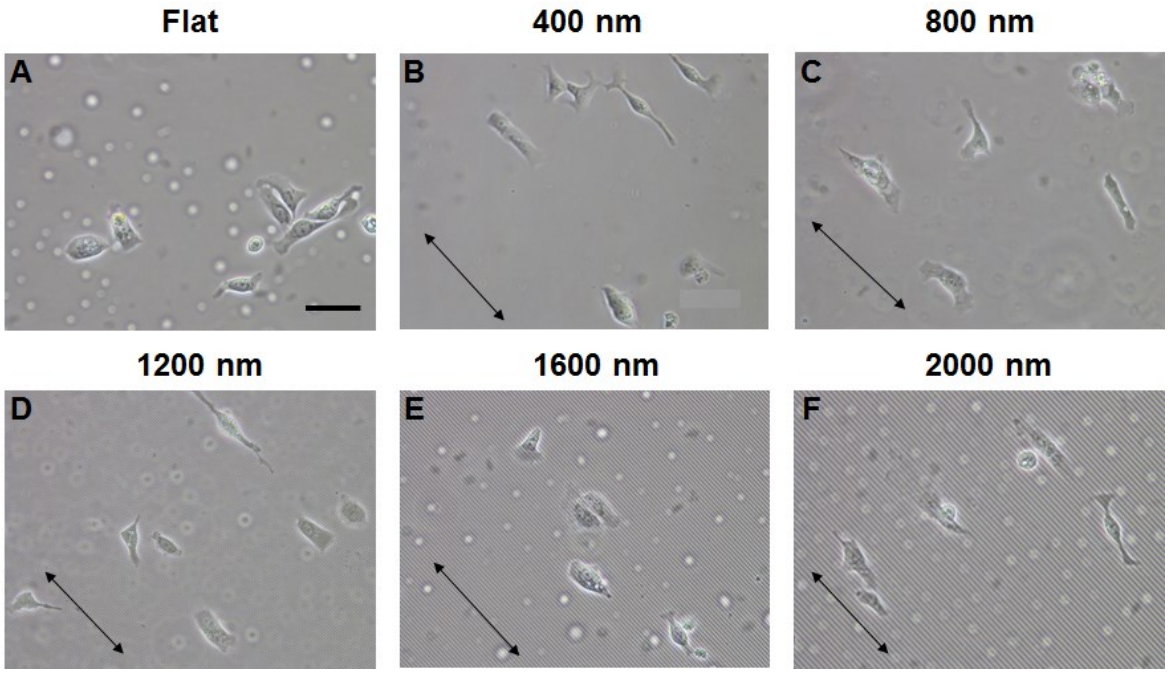

Figure 15. IMR90 cardio adhesion of PUABP2-RGD (100μM) coated 4x4 island patterns 24 hours post replating. Conditions include following nanogroove widths (A) flat, (B) 400nm, (C) 800nm, (D) 1200nm, (E) 1600nm, and (F) 2000nm. No significant differences in cell adhesion among pattern dimensions observed. Scale bar: 50μm.

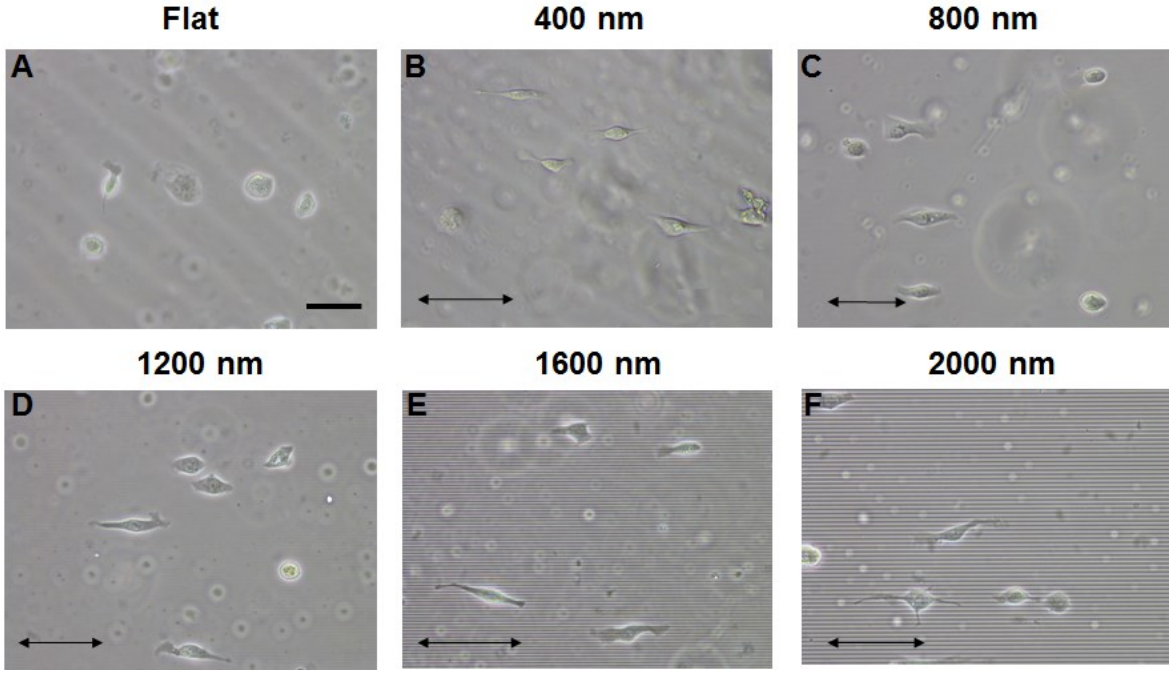

Figure 14. IMR90 cardio adhesion of PUABP1-RGD (100μM) coated 4x4 island patterns 24 hours post replating. Conditions include following nanogroove widths (A) flat, (B) 400nm, (C) 800nm, (D) 1200nm, (E) 1600nm, and (F) 2000nm. No significant differences in cell adhesion among pattern dimensions observed. Scale bar: 50μm.

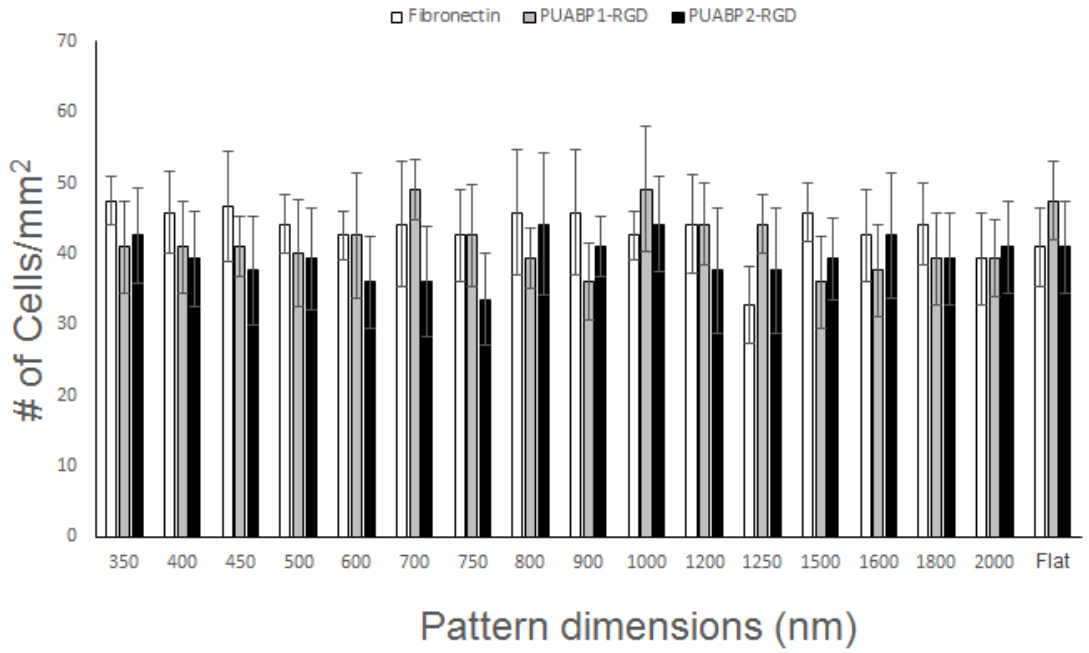

Figure 16. Cell adhesion of IMR90 cardios 24 hours post replating on 4x4 nanopattern platform coated with either fibronectin (50µg/ml), PUABP1-RGD (100µM), or PUABP2-RGD (100µM). Statistical analysis yielded no significant differences in cell adhesion among pattern dimensions and ECM coating. N = 20 (distinct areas) per condition.

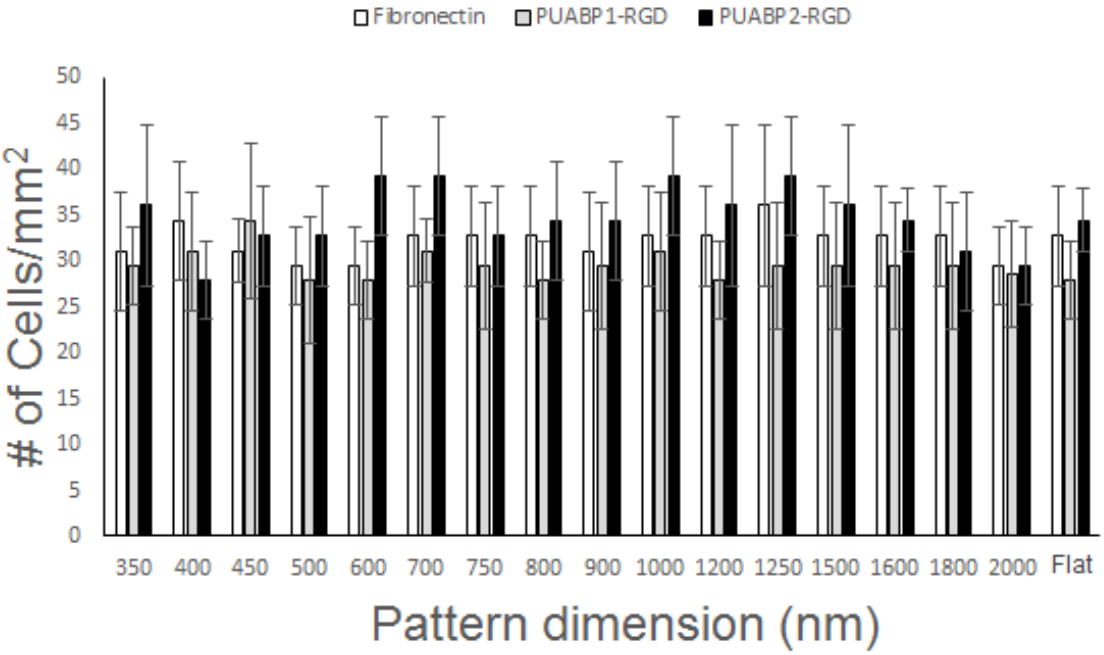

Figure 17. Cell adhesion of RUES2 cardios 24 hours post replating on 4x4 nanopattern platform coated with either fibronectin (50µg/ml), PUABP1-RGD (100µM), or PUABP2-RGD (100µM). Statistical analysis yielded no significant differences in cell adhesion among pattern dimensions and ECM coating. N = 20 (distinct areas) per condition.

CHAPTER 4: STRUCTURAL MATURATION OF SINGLE CELL HPSC-CMS

4.1 *Introduction*

Here we demonstrate the ability of the 4 x 4 island nanopattern to screen human pluripotent stem cell-derived cardiomyocyte structural maturation. The nanotopographic platform is combined with the bifunctional peptide PUABP-RGD to determine whether the addition of the ECM-mimicking molecule can influence phenotypic maturation of hPSC-CMs. First we display the ability of PUABP-RGD candidates to initiate cell adhesion, compared to standard ECM proteins (fibronectin). We then present morphological results which elucidates the combinatorial effect of nanogroove width and ECM-protein choice on human stem cell-derived cardiomyocytes maturation.

4.2 *Methods and Materials*

Fabrication of Nanopatterned Substrates

All NOA (Norland Optical Adhesive) substrate fabrication was accomplished by UV-assisted capillary force lithography. Prefabricated silicon masters (1st generation master) were used as the starting step in the fabrication of nanopatterned substrates. 40μL of PUA (poly(urethane acrylate)) 301 (19.8 MPa) was dropped dispensed on clean silicon master surface (100% ethanol or xylene and dry under O_2/N_2 gas). A sheet of 4cm x 4cm transparent polyester (PET) film was placed over the dispensed PUA. The silicon master, prepolymer, and PET were placed approximately 10cm below a 20 Watt (115V) UV light (λ = 365nm) for 50 seconds. The intensity of the light was 100mW/cm^2 at the surface of the substrate. After curing, the PET film was slowly removed with forceps. PUA should

attach to the PET film with a negative of the silicon master nanopattern. The PUA/PET nanopatterns were then cured under UV for at least 12 hours prior to use. The next step in the process involves using the 2nd generation master to pattern NOA substrates on glass slides that would be used for biological experiments. Glass slides were cleaned for 20min in isopropyl alcohol, ozone treated for 10 min, and coated with glass primer to increase adhesion of the NOA polymer to the surface. 10μl NOA polymer was drop dispensed on the pretreated glass slide and the nanopatterned master was placed face down on the polymer/glass surface. The glass slides (plus master) were UV cured for 50 seconds followed by peeling off the master from the glass surface (**Figure 3**). Protocol deviations for full patterns versus 4x4 island patterns only occurred in the original master fabrication. Island pattern masters were obtained from prefabricated 4x4 silicon masters (350nm – 2000nm) (**Figure 8)**.

hESC-CM Differentiation

RUES2 cardiomyocyte differentiation was accomplished using an established protocol. Replated human embryonic stem cells were induced with RPMI-B27 medium plus supplemental activin A (100ng/mL) at a volume of 1mL per well of a 24-well plate. After 24 hours the activin A containing medium was replaced with 1 mL of RPMI-B27 with supplemental BMP-4 and cultured for 4 days without medium change. At day 5, the BMP-4 containing medium was replaced with 1mL of RPMI-B27 medium. After day 5 cells are fed with RPMI-B27 medium every other day and monitored for spontaneous beating activity which reaches is peak around day 14. The differentiated cardiomyocytes are then fed until replating for *in vitro* experiments between days 18-20 **(Figure 11)**.

hiPSC-CM Differentiation

IMR90 cardiomyocyte differentiation was accomplished using a protocol established by James Thomson[13]. The protocol is similar to that of the directed differentiation of the RUES2 cardio cell line. In addition to serial application of activin A and BMP-4, cultures were supplemented with Wnt agonist CHIR 99021 in early stages and followed with Wnt antagonist Xav 939. The differentiated cardiomyocytes are then fed until replating for *in vitro* experiments between days 18-20 **(Figure 11)**.

Cell Culture

Human embryonic stem cell-derived cardiomyocytes (RUES2) and human induced pluripotent stem cell-derived cardiomyocytes (IMR90) were used for this study. In single cell experiments, cells were seeded at a density of 15,000 cells per cm^2. Culture medium (RPMI +B27 + Insulin) was changed every other day throughout the length of the experiment (2mL). Prior to cell seeding, substrates were coated with 750uL fibronectin (50ug/ml) or PUABP2-RGD (100uM) and incubated overnight at 37°C.

Morphological Analysis

Bright field images were obtained from cultures between 2-3 weeks after plating. 5-7 images were taking for each experimental condition to obtain sample size range of 25-40 cells. ImageJ (NIH) software was used to determine cell area, perimeter, major axis length, minor axis length, and orientation with respect to the direction of the pattern.

Immunostaining

Cells were fixed at the end of 2-3 weeks of culture with 4% paraformaldehyde (Affymetrix). Cells were then rinsed twice with PBS and permeabilized with .1% Triton-X-100 in PBS for twice for 5 minutes. Samples were then blocked with 1% bovine serum albumin (in PBS) for 40-60 minutes at room temperature. Primary antibodies were then diluted in 5% BSA: alpha-actinin 1:1000 (sigma Aldrich incubated for 1 hour at room temperature. Secondary antibodies were diluted in 5% BSA to match dilution of primary antibody dilution: Alexa Fluor-594 was used for alpha actin and conjugated Alexa-Fluor488/-Phalloidin was used for cytoskeleton staining. Samples were incubated at 37°C with secondary antibodies for 1 hr. Samples were then washed with PBS and prepared with VectaShield + DAPI and stored in 4°C until confocal imaging.

Statistical Analysis

All statistical analysis was performed using SigmaPlot ™. 2-way ANOVA tests were performed to determine statistically significant variances among experimental conditions, with post-hoc analysis performed to determine statistical differences between subgroups. A p value < .05 was considered to be statistically significant.

4.3 *Results/Discussion*

Cell Morphology

Here we report the effect of nanogroove width on morphology of human stem cell derived cardiomyocytes (3 weeks post-replating). It was previously reported that the width of the grooves affects the ability of the cell body to penetrate and structurally mature[23]. The

ability of a cell to penetrate the grooves of nanogrooves determines the degree to which a cell will elongate and align with the underlying pattern. The influence of the pattern is expected to push cells towards a more adult phenotype. However, as cells are less able to penetrate into smaller groove widths, the influence of the topography becomes less apparent. Cells seeded on much large nanogroove widths are expected to encounter several problems which inhibit their ability to structural mature. As the widths become extremely large cells can become isolated on grooves or in ridges; the section of the cell that interacts with the underlying substrate is not able to differentiate a topography as it only comes into contact with the surface of a ridge (appears flat) or may become overly entrenched within a groove. Images were taken at 3 weeks post-replating to evaluate the effect of nanogroove width and ECM composition on structural maturity (**Figures 18-21**). Structural maturity was evaluated by analyzing cell area, perimeter, circularity, and anisotropy.

Cell area measurements for both cell lines yielded trends that followed expectations outlined above. Both cell types exhibited enlarged areas on nanopatterns ranging between 700 – 1000nm (**Figures 22, 23**). Group statistical analysis via 2-way ANOVA indicated variances between experimental conditions with $p < .05$. Post-hoc analysis between specific groups indicated statistically significant differences in cell area, an important structural indicator of hPSC-CM maturation. Cell area on 800nm wide nanopatterns was significantly larger than cell area on 350nm, 1500nm, 2000nm, and flat controls (chosen for comparison). Much smaller deviations were observed between cell area on 350nm and 2000nm and flat controls. The mechanism by which cell area is reduced on the outer may be dimension, but observations suggest that they are less

conducive to maturation of hPSC-CM phenotype. Interestingly, similar trends were observed with cultures that were precoated with PUABP2-RGD. There was not a significant difference in cell area between fibronectin and PUABP2-RGD. This finding is important because it points to the long term viability of PUABP2-RGD in hPSC-CM cultures.

Cell Perimeter is another structural cardiac maturity marker as perimeter is representative of hypertrophy. As was seen with analysis of cell area, results displayed a trend towards intermediate nanopattern dimensions as indicators of increased cell perimeter (**Figures 24, 25**). This result was expected based on cell area findings, as cell area and perimeter sizes are strongly associated. Cell perimeters varied significantly between 800nm and 350nm, 1500nm, 2000nm, and flat controls. Perimeters were similar between 350nm, 2000nm, and flat controls. Again, cells cultured on PUABP2-RGD coated substrates elicited results similar to those coated with fibronectin. Statistical analysis revealed variances between fibronectin and PUABP2-RGD, but the variations were isolated to 1-2 dimensions (1500nm (IMR90 cardios), 750nm/1600nm (RUES2 cardios)).

Circularity is essentially a measure of how elongated a cell becomes. A circularity of index of 1 indicates a perfect circle and a circularity index of 0 indicates a straight line. Thus, circularity becomes an important analytical tool when determining structural maturity of stem cell-derived cardiomyocytes. The single adult cardiomyocyte exhibits a square-like elongated cell body with organized myofibrils while immature cardiomyocytes are much more rounded with disorganized myofibrils. Therefore, we can use cell elongation as another aspect of structural maturity (**Figures 26, 27**).

Evaluation of the circularity index of single hPSC-CMs yielded results further supporting improved structural maturity of intermediate pattern dimensions. For both cell lines, on fibronectin and PUABP2-RGD, the circularity index was significantly reduced on 800 nm in comparison to 350nm, 2000nm, and flat controls. This was consistent with expectations as cells on outer dimensions are not able to interact with the nanogrooves to the same degree as those in intermediate ranges. Interestingly, statistical analysis revealed significant variances between fibronectin and PUABP2-RGD circularity indices, on outer pattern dimensions. However, there were not significant differences between ECM coating types on 800nm. Although further investigation would be necessary to explain the differences between circularity index on outer dimension, one potential explanation is that the peptide immobilization on to the surface of outer dimensions may be less uniform.

A promising takeaway for the analysis of the circularity index is the drastically reduced circularity on 800nm patterns compared to flat controls at the 3 week time point. Lundy *et al*.[7] reported a similar reduction in circularity based on culture length. Late stage (~100 day) circularity measurements are similar to those found in our analysis of cells on 800nm patterned substrates at 3 weeks (40~ days post-replating). It is clear that the presences of underlying ECM topography promotes improved structural aspects of hPSC-CM maturity.

Cell orientation was also evaluated as a measure of the degree to which cells interact with the underlying patterns (**Figures 28, 29**). It is expected that the ability of cells to penetrate into nanogrooves will strongly influence whole cell alignment. To evaluate cell alignment the angle between the major axis of the cell and the underlying pattern was

measured. All measurements per condition were compiled and the percentage of cells within 10 degrees of the underlying pattern was computed.

As was expected, the highest percentage of cells falling within 10 degrees of the pattern direction was around 800nm. Cell alignment was significantly higher on 800nm patterned substrates when compared to cells on 350nm, 1500nm, 2000nm, and flat controls. As mentioned, this was expected based on the hypothesis that the degree to which a cell can penetrate into grooves will influence overall cell alignment. On smaller widths cells are less able to protrude into nanogrooves, inhibiting the nanogrooves from aiding in alignment of the cell. Widths of the patterns at the larger end of the spectrum have a lower influence on cell alignment because of the inability of cells to sense the presence of underlying grooves. Major portions of the cell become isolated on ridges or within grooves inhibiting tight protrusions of the cell into those grooves and thus become less influenced by the orientation of the pattern. Again, the data suggests a significant difference between cell alignment of the fibronectin and RGD conditions when reaching larger pattern dimensions. Further investigation will be required to explain this as the potential mechanisms creating the deviation are not very well understood.

Immunostaining:

Samples were fixed at 3 weeks and stained with alpha-actinin (sarcomere analysis), F-actin (cytoskeleton alignment), and DAPI (nucleus) (**Figure 30-31**). Stained images also provided qualitative representations of differences of cell morphology across dimensions. Interestingly, on the 800nm substrates sarcomere structures were visibly more well organized, and corresponding myofibrils, than outer pattern dimensions and

the flat control. Cells fixed on 800nm also displayed more densely packed fibrils and higher overall amount compared to smaller and larger dimensions.

The key piece of information obtained from immunostained images was the sarcomere length within cells on each of the pattern dimensions. Sarcomere length is directly related to force production from cell contractions. Sarcomere length can be essentially correlated to the frank-starling law on a nanoscale. Increased sarcomere length relates to the amount myosin heads can slide along actin filaments to perform forceful contractions. It has been reported that adult cardiomyocytes have sarcomere lengths in the region of 2.1-2.3 microns while immature cardiac cells often have sarcomere lengths of approximately 1.5 microns[7].

Sarcomere analysis yielded very promising results (**Figure 32**). We report maximum sarcomere length in cells on intermediate pattern dimensions. There was a significantly significant increase in sarcomere length in cells on 800nm patterns in comparison to cells on 350nm, 1500nm, 2000nm, and flat controls. The sarcomere length of cells on 800nm substrates was approximately 1.85 microns (+- .056) which is a significant increase in length compared to other studies on hPSC-CMs of similar age[7]. It is hypothesize that the presence of the underlying pattern of ideal dimensions can promote structural organization of the internal cytoskeleton which leads to improved sarcomere organization and length. The aid of the underlying ECM essentially expedites the structural maturation of the cardiomyocytes compared to those cultured on flat controls. It is important to note that the same trends in sarcomere length were observed on samples precoated with PUABP2-RGD. As similar trends were observed in other

morphological analysis it is promising to observe that PUABP2-RGD samples can comparably mature the base contraction unit of human stem cell derived cardiomyocytes.

4.4 *Summary*

In summary, this study presented a platform in which different nanogroove widths could be screened for effects on hPSC-CM structural maturation. The study included evaluation of a bifunctional cell adhesion peptide PUABP2-RGD as an alternative to commonly used cell adhesion proteins such as fibronectin for hPSC-CM structural maturation. Morphological analysis of samples at 3 weeks post-replating pointed to an intermediate range of nanogroove widths as the most beneficial to maturation of structural characteristics. Statistical analysis was performed to determine significant variations between cell morphology on 350nm, 800nm, 1000nm, 1500nm, 2000nm, and flat controls. It was determined that cells on 800nm had significantly larger cell areas, larger perimeters, reduced circularity, and improved anisotropy compared to the other analyzed dimensions. It was also shown that sarcomere length on 800nm was significantly greater than the other pattern dimensions. It was hypothesized that the results would be observed based on the ability of the cell body to penetrate in the grooves of the nanopattern. Smaller pattern widths inhibited optimal penetration of cells which rendered the underlying ECM less influential. On larger pattern dimensions the increased width between adjacent grooves and ridges isolated large portions of the cell body, making it appear comparable to a flat surface.

It was also found that the custom made bifunctional peptide, PUABP2-RGD, performed significantly similar to fibronectin for cell adhesion and cell maturation

experiments. This is important, especially when considering transition to tissue level engineering as the synthesized peptide was specifically synthesized to have a high affinity for the substrate surface. Theoretically, this means that the surface coverage of the adhesion peptide would have higher uniformity and thus lead to improved monolayer formation in comparison to standard adhesion proteins. We demonstrated the clear influence of nanopatterned dimensions on structural maturity of human stem cell-derived cardiomyocytes. Ongoing work aims to evaluate functional maturation of hPSC-CMs on the platform described in the study.

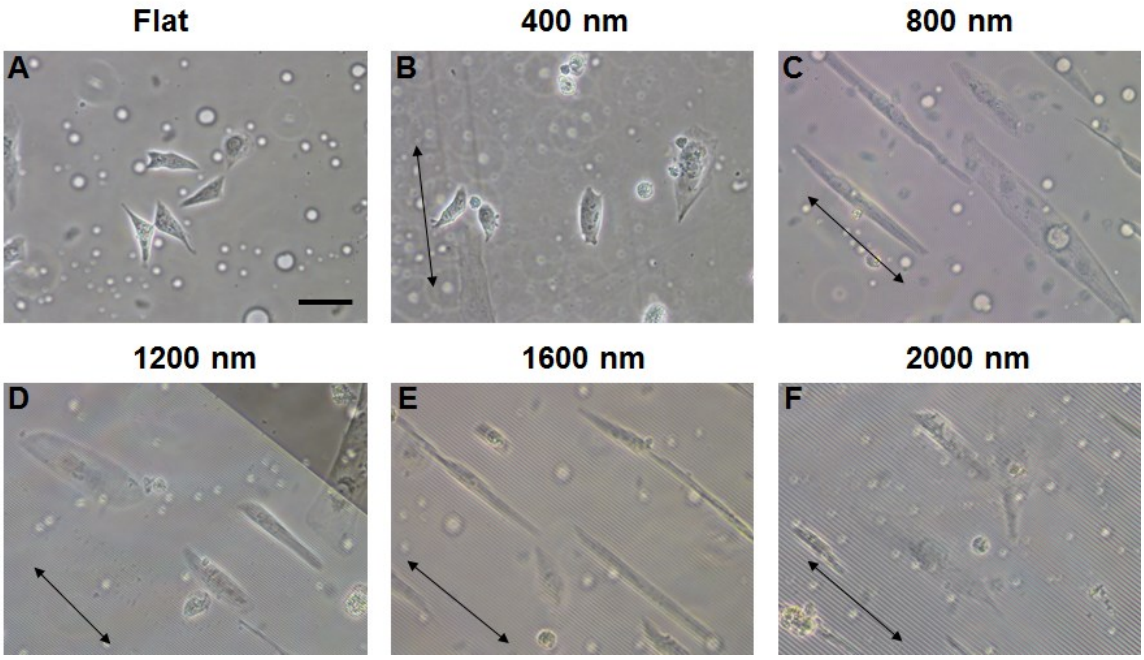

Figure 18. Phase contrast images of IMR90 cardios 3 weeks post replating on fibronectin (50µg/ml) coated 4x4 platform with following dimensions: (A) Flat, (B) 400nm, (C) 800nm, (D) 1200nm, (E) 1600nm, and (F) 2000 nm. Cell morphology displays increased elongation and hypertrophy of cells on 800nm nanogroove widths compared to other groove widths. Scale bar: 50µm.

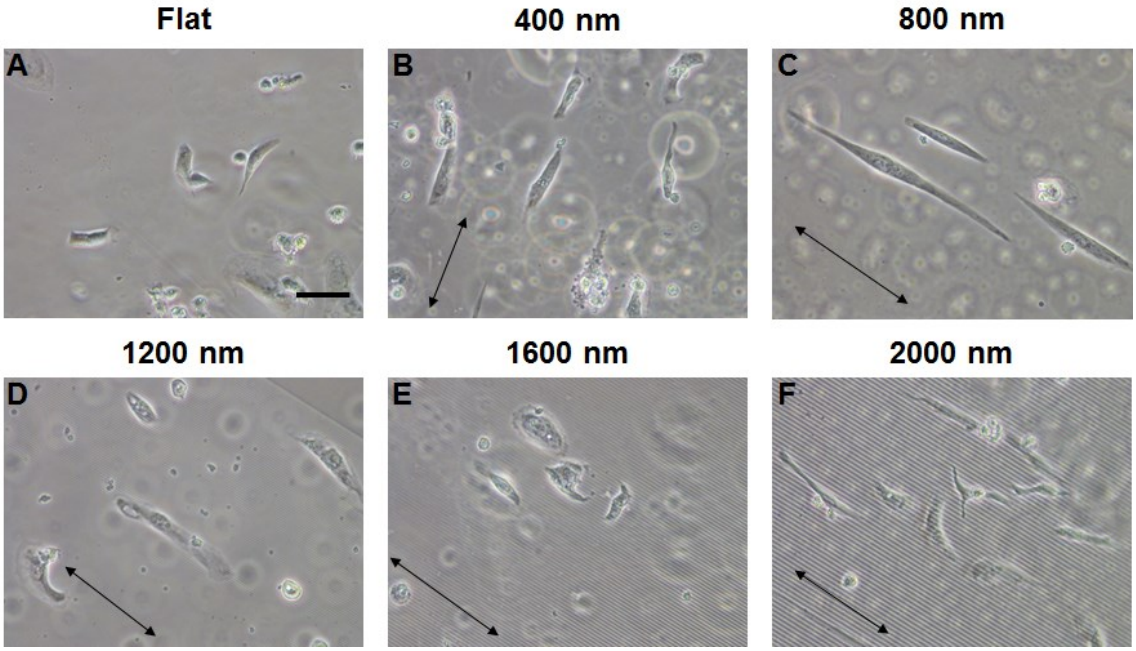

Figure 19. Phase contrast images of IMR90 cardios 3 weeks post replating on PUABP2-RGD (100µM) coated 4x4 platform with following dimensions: (A) Flat, (B) 400nm, (C) 800nm, (D) 1200nm, (E) 1600nm, and (F) 2000nm. Cell morphology displays increased elongation and hypertrophy of cells on 800nm nanogroove widths compared to other groove widths. Scale bar: 50µm.

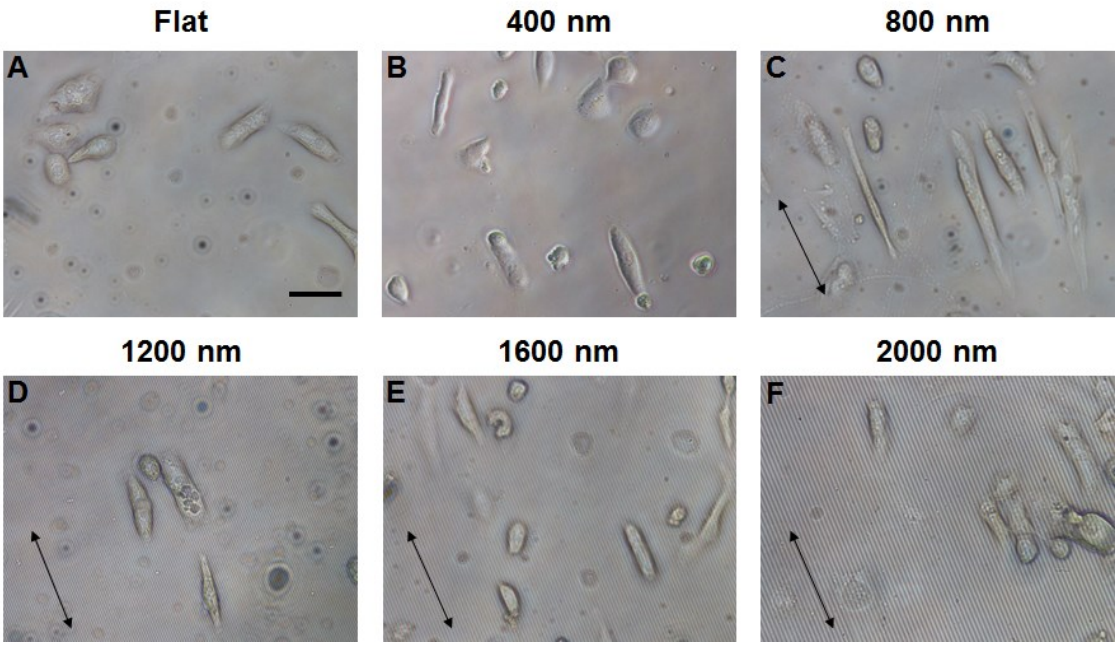

Figure 20. Phase contrast images of RUES2 cardios 3 weeks post replating on fibronectin (50µg/ml) coated 4x4 platform with following dimensions: (A) Flat, (B) 400nm, (C) 800nm, (D) 1200nm, (E) 1600nm, and (F) 2000nm. Cell morphology displays increased elongation and hypertrophy of cells on 800nm nanogroove widths compared to other groove widths. Scale bar: 50µm.

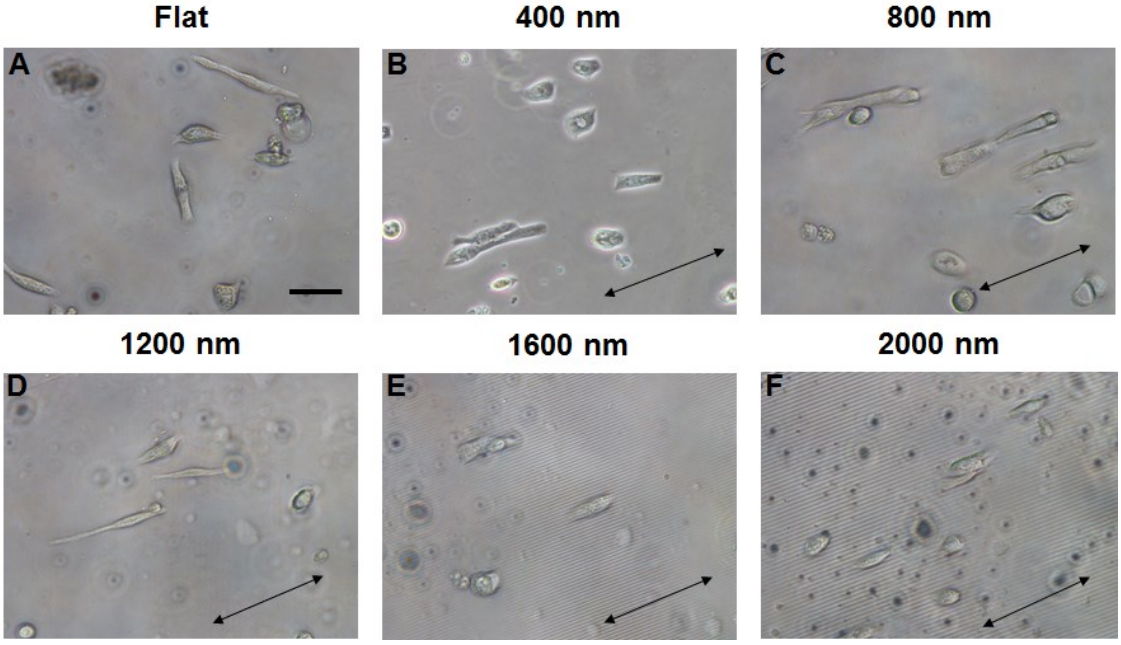

Figure 21. Phase contrast images of RUES2 cardios 3 weeks post replating on PUABP2-RGD (100µM) coated 4x4 platform with following dimensions: (A) Flat, (B) 400nm, (C) 800nm, (D) 1200nm, (E) 1600nm, and (F) 2000nm. Cell morphology displays increased elongation and hypertrophy of cells on 800nm nanogroove widths compared to other groove widths. Scale bar: 50µm.

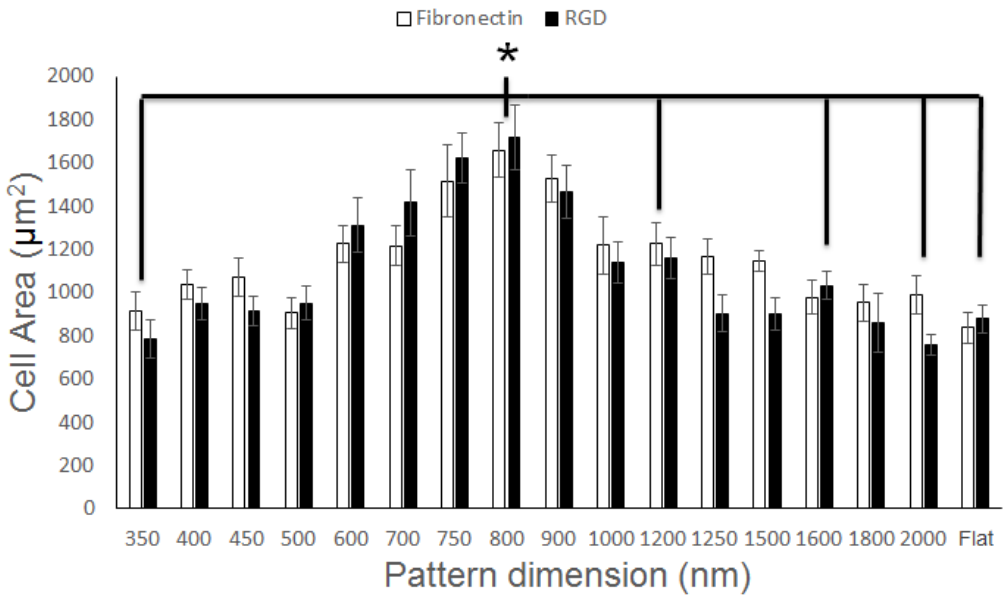

Figure 22. Cell area analysis of IMR90 cardios 3 weeks post replating pattern dimensions from 4x4 island platform with fibronectin (50µg/ml) and PUABP2-RGD (100µM). 2-way ANOVA statistical analysis indicated variance among the population, p< .05. Post host analysis determined statistically significant increase in cell area for cells on 800nm groove widths compared to those on 400nm, 1200nm, 1600nm, 2000nm, and flat controls (For both fibronectin and PUABP2-RGD). N = 25-40 cells per condition.

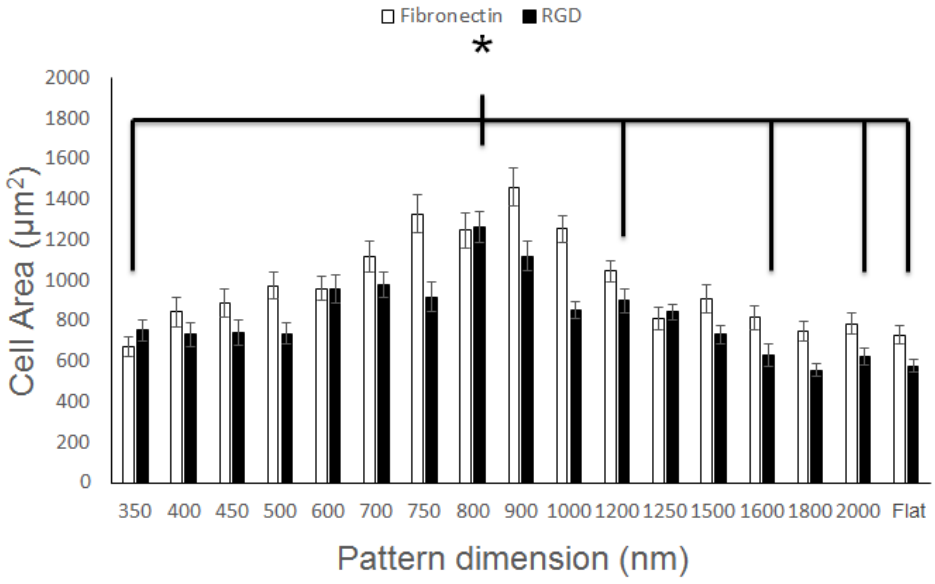

Figure 23. Cell area analysis of RUES2 cardios 3 weeks post replating pattern dimensions from 4x4 island platform with fibronectin (50µg/ml) and PUABP2-RGD (100µM). 2-way ANOVA statistical analysis indicated variance among the population, p< .05. Post host analysis determined statistically significant increase in cell area for cells on 800nm groove widths compared to those on 400nm, 1200nm, 1600nm, 2000nm, and flat controls (For both fibronectin and PUABP2-RGD). N = 25-40 cells per condition.

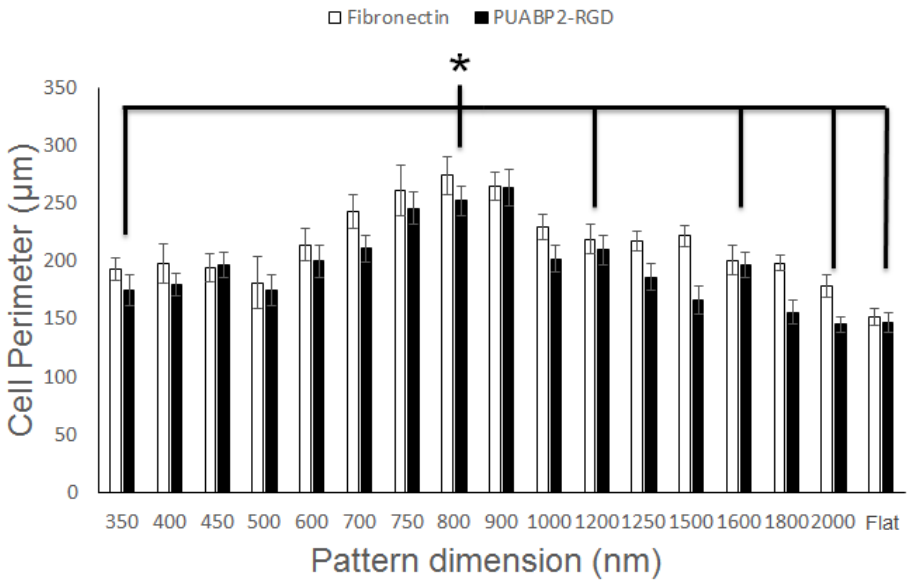

Figure 24. Cell perimeter analysis of IMR90 cardios 3 weeks post replating pattern dimensions from 4x4 island platform with fibronectin (50µg/ml) and PUABP2-RGD (100µM). 2-way ANOVA statistical analysis indicated variance among the population, p< .05. Post host analysis determined statistically significant increase in cell perimeter for cells on 800nm groove widths compared to those on 400nm, 1200nm, 1600nm, 2000nm, and flat controls (For both fibronectin and PUABP2-RGD). N = 25-40 cells per condition.

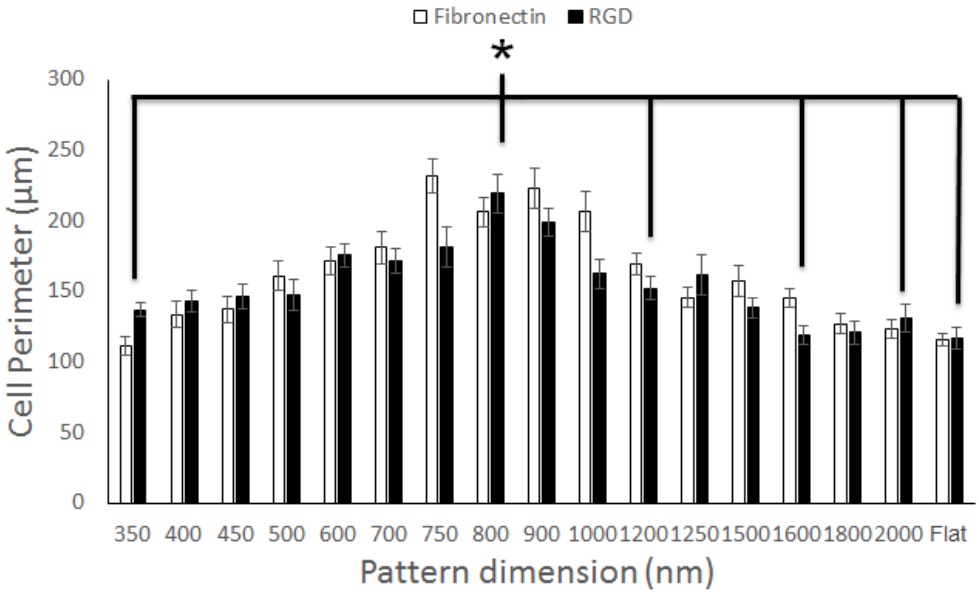

Figure 25. Cell perimeter analysis of RUES2 cardios 3 weeks post replating pattern dimensions from 4x4 island platform with fibronectin (50µg/ml) and PUABP2-RGD (100µM). 2-way ANOVA statistical analysis indicated variance among the population, p< .05. Post host analysis determined statistically significant increase in cell perimeter for cells on 800nm groove widths compared to those on 400nm, 1200nm, 1600nm, 2000nm, and flat controls (For both fibronectin and PUABP2-RGD). N = 25-40 cells per condition.

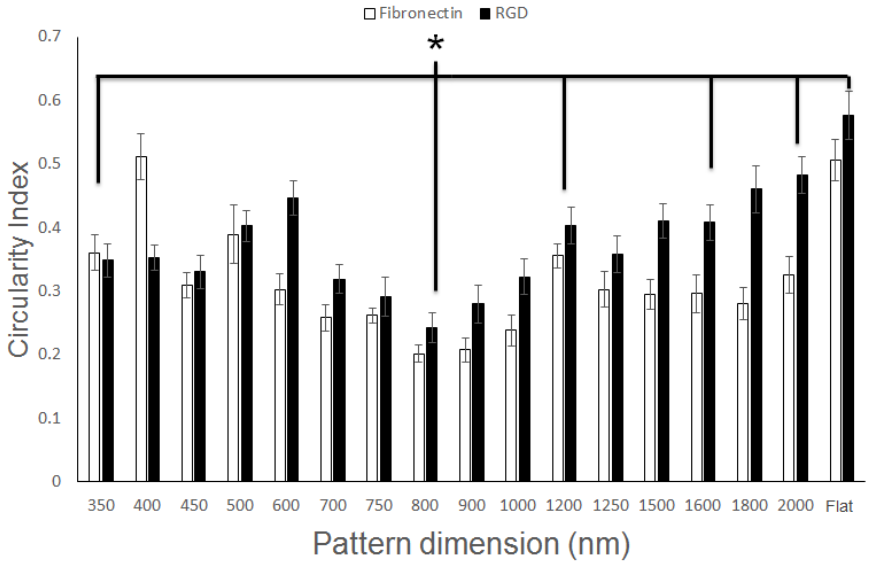

Figure 26. Cell circularity analysis of IMR90 cardios 3 weeks post replating pattern dimensions from 4x4 island platform with fibronectin (50µg/ml) and PUABP2-RGD (100µM). 2-way ANOVA statistical analysis indicated variance among the population, p< .05. Post host analysis determined statistically significant reduction of circularity index for cells on 800nm groove widths compared to those on 400nm, 1200nm, 1600nm, 2000nm, and flat controls (For both fibronectin and PUABP2-RGD). N = 25-40 cells per condition.

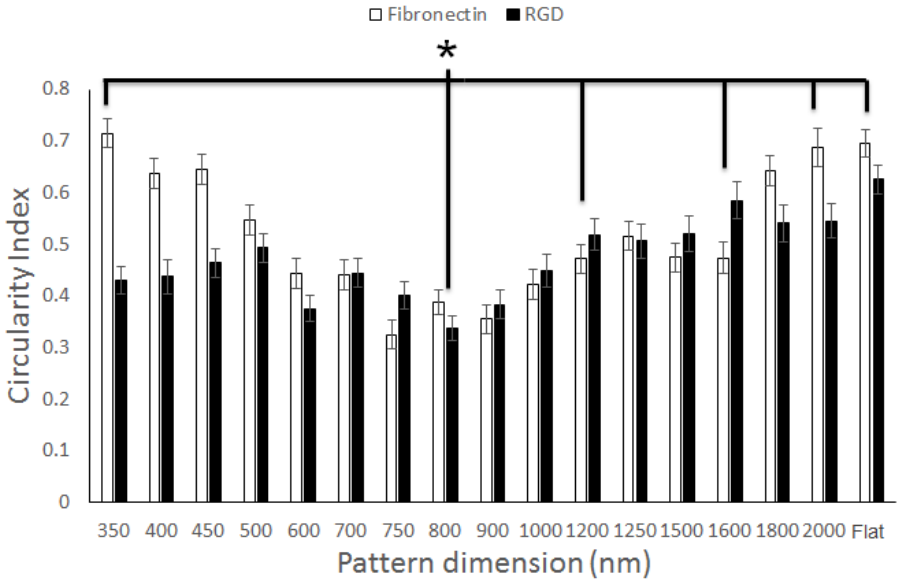

Figure 27. Cell circularity analysis of RUES2 cardios 3 weeks post replating pattern dimensions from 4x4 island platform with fibronectin (50µg/ml) and PUABP2-RGD (100µM). 2-way ANOVA statistical analysis indicated variance among the population, p< .05. Post host analysis determined statistically significant reduction of circularity index for cells on 800nm groove widths compared to those on 400nm, 1200nm, 1600nm, 2000nm, and flat controls (For both fibronectin and PUABP2-RGD). N = 25-40 cells per condition.

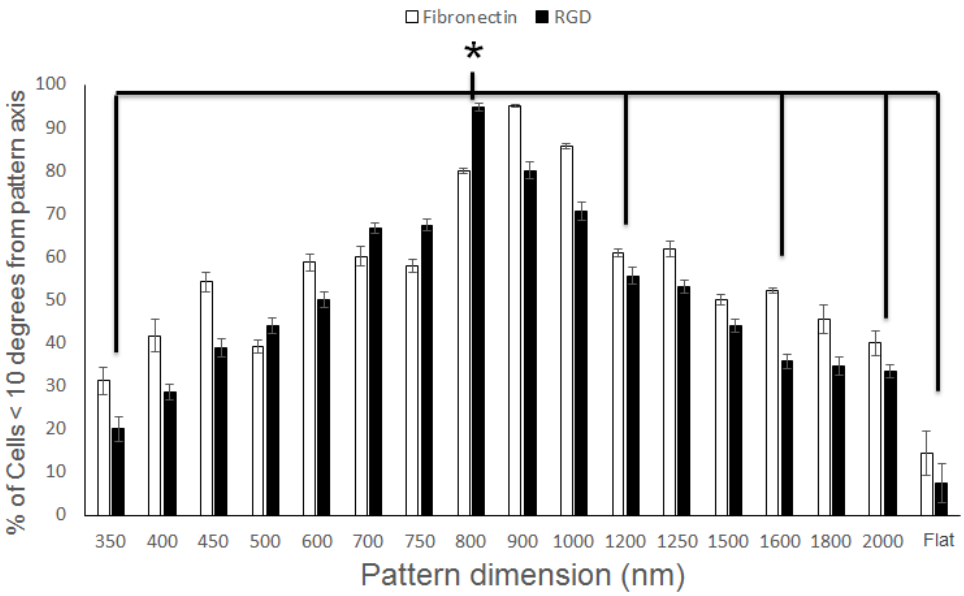

Figure 28. Cell alignment analysis of IMR90 cardios 3 weeks post replating pattern dimensions from 4x4 island platform with fibronectin (50µg/ml) and PUABP2-RGD (100µM). Alignment was determined by the percentage of cells whose major axis was within 5 degrees of groove direction. 800nm nanogroove width exhibited higher degree of cell alignment compared to 400nm, 1200nm, 1600nm, 2000nm, and flat controls (For both fibronectin and PUABP2-RGD). N = 25-40 cells per condition.

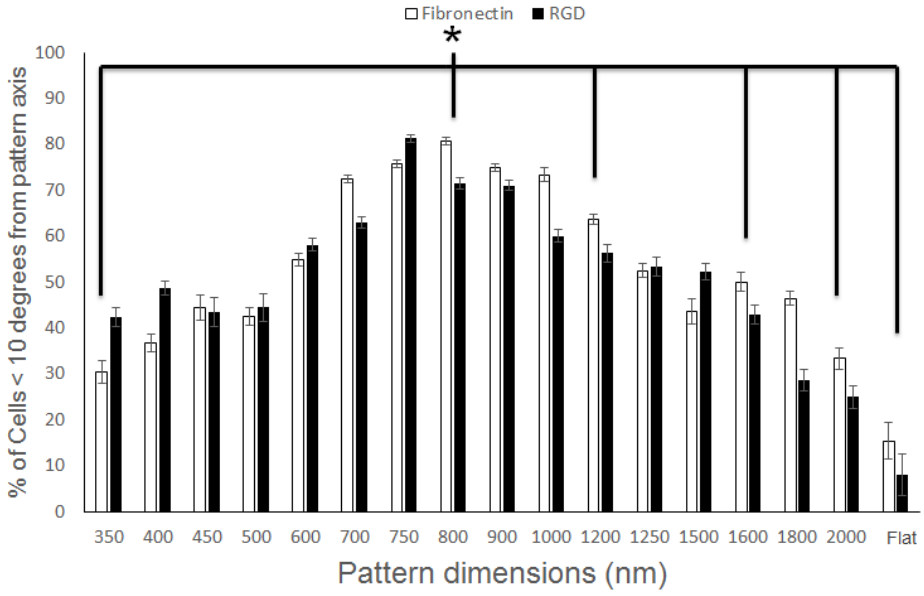

Figure 29. Cell alignment analysis of RUES2 cardios 3 weeks post replating pattern dimensions from 4x4 island platform with fibronectin (50µg/ml) and PUABP2-RGD (100µM). Alignment was determined by the percentage of cells whose major axis was within 5 degrees of groove direction. 800nm nanogroove width exhibited higher degree of cell alignment compared to 400nm, 1200nm, 1600nm, 2000nm, and flat controls (For both fibronectin and PUABP2-RGD). N = 25-40 cells per condition.

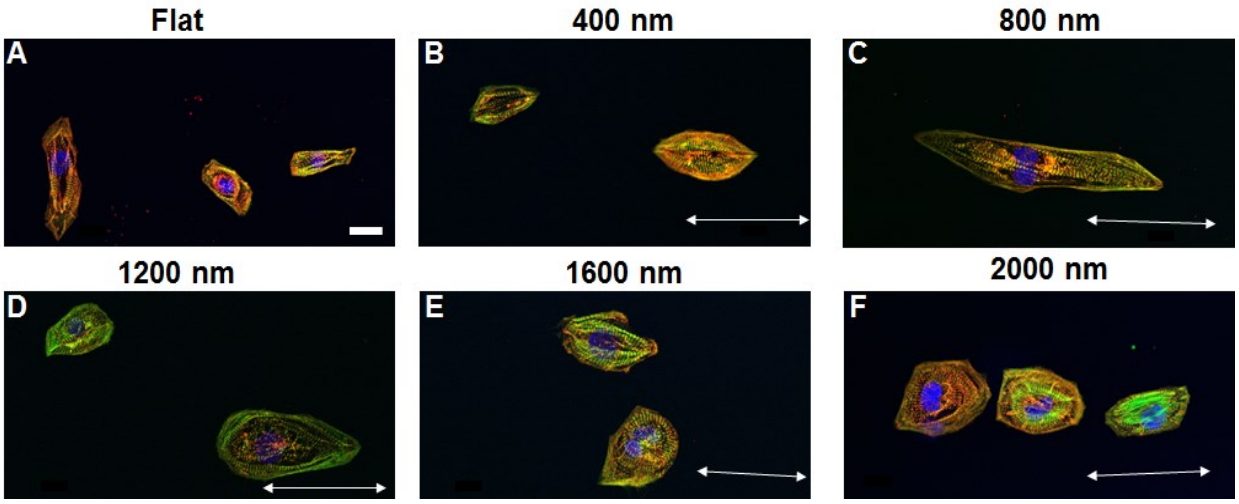

Figure 30. Confocal images of IMR90 cardios fixed 3 weeks post replating on fibronectin (50µg/ml) coated 4x4 platform with following dimensions: (A) Flat, (B) 400nm, (C) 800nm, (D) 1200nm, (E) 1600nm, and (F) 2000 nm. Cell morphology displays increased elongation, hypertrophy, and improved sarcomere organization of cells on 800nm nanogroove widths compared to other groove widths. Red = alpha-actinin, Green = f-actin, Blue = DAPI. Scale bar: 20µm.

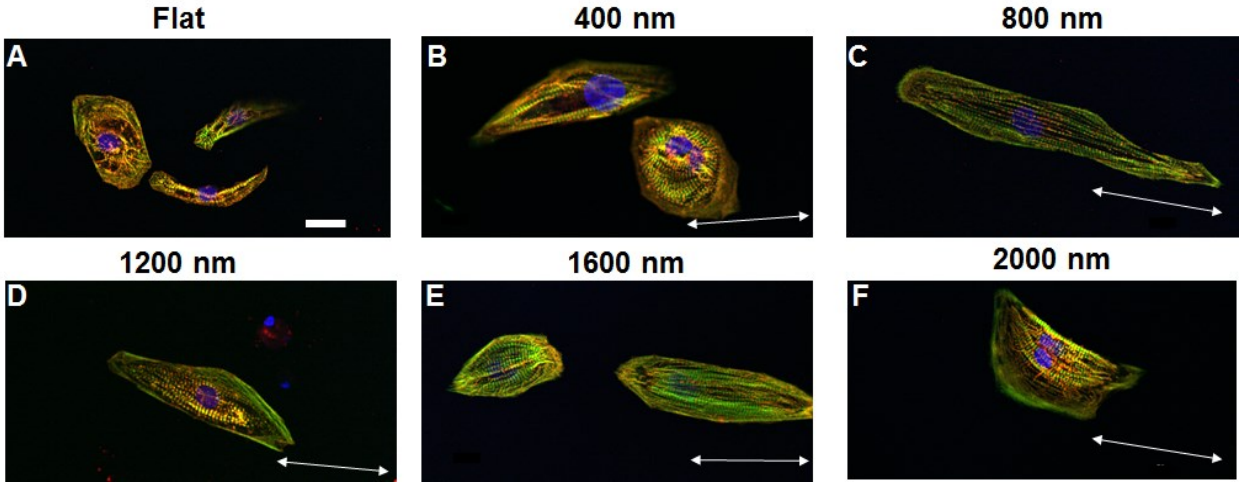

Figure 31.Confocal images of IMR90 cardios fixed 3 weeks post replating on PUABP2-RGD (100µM) coated 4x4 platform with following dimensions: (A) Flat, (B) 400nm, (C) 800nm, (D) 1200nm, (E) 1600nm, and (F) 2000 nm. Cell morphology displays increased elongation, hypertrophy, and improved sarcomere organization of cells on 800nm nanogroove widths compared to other groove widths. Red = alpha-actinin, Green = f-actin, Blue = DAPI. Scale bar: 20µm.

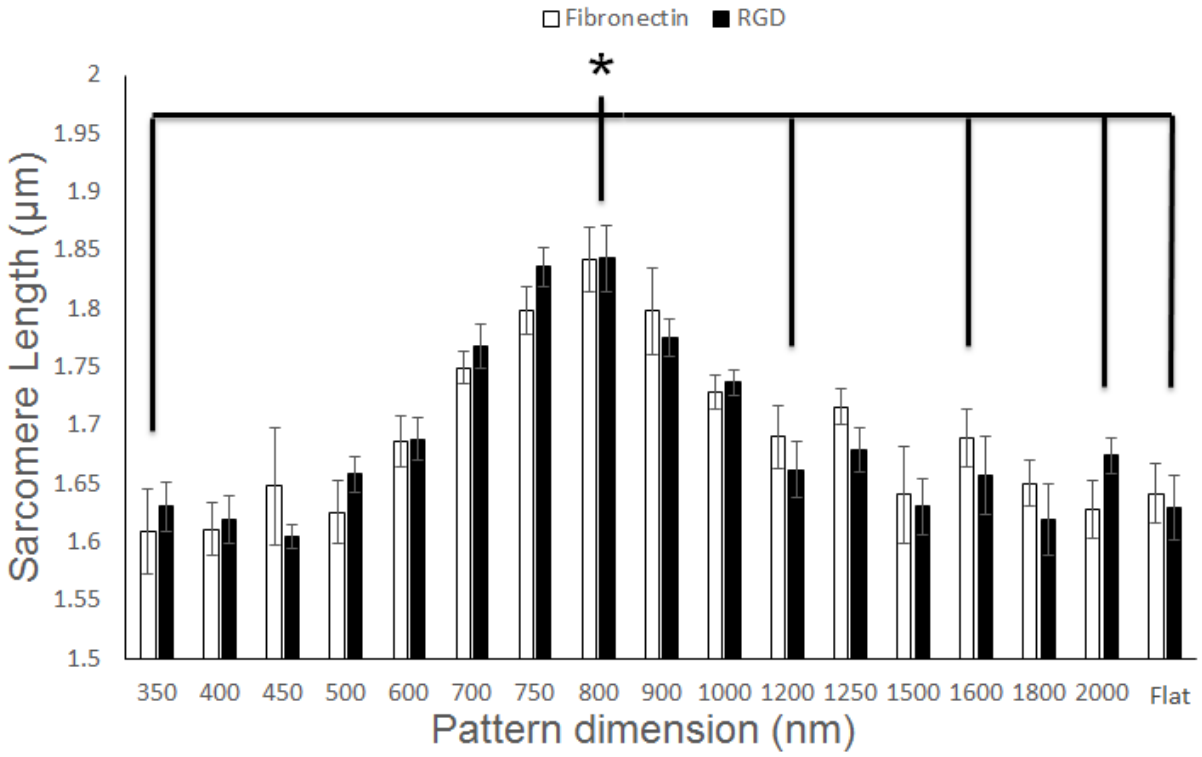

Figure 31. Sarcomere length analysis of IMR90 cardios 3 weeks post replating pattern dimensions from 4x4 island platform with fibronectin (50µg/ml) and PUABP2-RGD (100µM). 2-way ANOVA statistical analysis indicated variance among the population, $p < .05$. Post host analysis determined statistically significant increase in sarcomere length for cells on 800nm groove widths compared to those on 400nm, 1200nm, 1600nm, 2000nm, and flat controls (For both fibronectin and PUABP2-RGD). N = 25-35 cells per condition.

CHAPTER 5: CONCLUSIONS

First we report the development of a combinatorial platform that can be used to assess the effect of different nanoscale dimensions as well as different ECM composition on structural and functional maturation of hPSC-CMs. We then go on to demonstrate the effect of differential nanoscale dimensions on structural maturation of human stem cell derived cardiomyocytes. Through analysis of nanogroove dimensions ranging from 350nm – 2000nm we identified a smaller range, or "sweet spot," in which the nanogroove width allowed for ideal cell penetration and thus improved structural maturity of hPSC-CMs. The results suggest that the dimensions of the underlying ECM-like substrate is an important factor to consider when designing *in vitro* engineered cardiac tissue. We also identified the bifunctional peptide PUABP2-RGD as a viable alternative to cell adhesion proteins such as fibronectin and laminin. Overall, results suggested comparable cell adhesion and cell morphology between substrates coated with fibronectin and PUABP2-RGD. Although these findings provide promising insight into the role of ECM biochemical and biomechanical influences on cardiac cell maturation, it will be important to also elucidate the effect of ECM influences on hPSC-CM function *in vitro* as the ultimate goal is to engineered native-like functional myocardium.

The role of ECM cues was briefly investigated in 2-D hPSC-CM monolayers. Through structural and functional evaluation, nanotopography as well as substrate rigidity were tested for human induced stem cell-derived cardiomyocyte monolayers (results not shown). The results suggested no apparent differences between substrate rigidities and topography compared to flat controls (results not shown). One main limitation may have played an important part in the findings displayed from these studies; the ability to develop

reproducible monolayers remains to be a clear challenge. The tendency for hiPSCs to aggregate can yield the potential influence of the underlying substrate ineffective. As promising results have been observed on single cell analysis through the incorporation of PUABP2-RGD, future work may benefit from immobilized peptide incorporation to engineered cardiac tissues *in vitro*. This has also prompted ongoing work to develop and implement alternative substrate materials that have been widely used in cardiac tissue engineering (PEG-DA)[35-37].

It is important that the future of the study focuses on obtaining functional data from the single cell experiments. This includes contractility measurements as well as calcium handling. During this study attempts were made to acquire functional data, but technical limitations prevented meaningful results. Specifically, calcium imaging was difficult to acquire because of the working distance of the confocal microscope. It will be necessary to alter the method in which the 4x4 platform is setup to ensure that higher magnifications can be used to acquire a significant calcium signal. Contraction measurements will also require an alternative approach as it is not feasible to use the IonOptix system; it is not feasible because the system operates based on differences in light contrast and the diffraction associated with nanopatterns makes it difficult to establish cell borders.

It would be interesting to study the effect of different substrate rigidities in combination with the differential nanoscale topographies and adhesion molecules. Preliminary studies have been attempted, but further analysis should be able to elucidate the effect of ECM stiffness on single cell function. While many papers state that substrate rigidities should be studied in more physiological ranges (10-50kPa), they fail to realize that these rigidities are associated with the tissue itself and not the underlying ECM which

reach much higher rigidities. It would also be interesting to further investigate the role the outlined experimental conditions play on cell adhesion mechanisms. Evaluation of integrin formation may provide insight into the cell adhesion process. Staining of vinculin can also provide results displaying the maturation and formation of cell-ECM complexes.

The main limitation associated with 2-D human stem cell-derived cardiomyocyte monolayer study was the reproducibility and maintenance of an intact cell monolayer. The migratory behavior of the cells in a monolayer and the desire to aggregate may be result of immature cell-ECM integrins in comparison to cell-cell integrins. It would be beneficial to test the binding peptide developed in this study on cell monolayers to determine if it can improve overall ECM surface coating and cell adhesion. It will be important to gather further characterization data of the PUABP-RGD molecule to highlight improved surface coverage and peptide immobilization compared to fibronectin (or related ECM proteins). This can be achieved by AFM surface characterization of flat surfaces coated with PUABP2-RGD and fibronectin. Theoretically, a uniform increase in surface thickness will be seen as the PUABP2-RGD disperses and immobilizes to the substrate. In comparison, it would be expected that suboptimal immobilization of the fibronectin protein will yield only patches of increased thickness. One study to evaluate the potential benefit of the bifunctional peptide will focus on long term maintenance of monolayers of cardiac tissue seeded on scaffolds with PUABP-RGD versus fibronectin. Evaluation of the tendency of monolayers to aggregate over time can effectively highlight the difference in cell-ECM adhesion strength between different coating materials (PUABP-RGD, fibronectin). Lastly, investigation of alternative substrate materials may result in improved

monolayer reproducibility and thus improved potential to mature human stem cell-derived cardiomyocyte phenotype.

VITA

Daniel Sinclair Carson was born and raised in Anchorage, Alaska. He earned a Bachelor's in Bioengineering from the University of Washington in 2012. He earned a Master's in Bioengineering from the University of Washington in 2013.

References

1. Khatayevich, Dmirtiy; Gungormus, Mustafa *et al.* “Biofunctionalization of materials for implants using engineered peptides.” *Acta Biomaterialia.* Vol. 6, pp. 4634-46-41, 2010.
2. Ruoslahti, Erkki. “RGD and other recognition sequences for integrins.” *Annual Review of Cell and Developmental Biology.* Vol. 12, pp. 697-715, 1996.
3. Kreutziger, K. L.; Murry, C. E. "Engineered Human Cardiac Tissue." *Pediatric Cardiology.* pp. 334-341, 2011.
4. Fact Sheet: The Top 10 Causes of Death. World Health Organization. Nov. 2008. Retrieved
5. Fact Sheet: “International Cardiovascular Disease Statistics.” American Heart Association, 2004.
6. Bolooki, Michael,; Askari, Arman. "Disease Management Project: Acute Myocardial Infarction." *Cleveland Clinic*. Cleveland Clinic, 2011. Web. 10 Mar. 2013.
7. Lundy, Scott D.; Zhu, Wei-Zhong *et al.* “Structural and Functional Maturation of Cardiomyocytes Derived from Human Pluripotent Stem Cells.” *Stem Cells and Development.* Vol. 22, no.14, pp. 1991-2002, 2013.
8. Segers, VFM; Lee, RT. “Stem-cell therapy for cardiac disease.” *Nature.* Vol. 451, pp. 937–942, 2008.
9. Bernstein, HS; Srivastava, D. “Stem cell therapy for cardiac disease.” *Pediatric Research.* Vol. 71, pp. 491–499, 2012.
10. Liau, B.; Christoforou, N. *et al.* “Pluripotent stem cell-derived cardiac tissue patch with advanced structure.” *Biomaterials.* pp. 9180-9187, 2011.
11. Becker, A. “Cytological Demonstration of the Clonal Nature of Spleen Colonies Derived from Transplanted Mouse Marrow Cells”. *Nature*. pp. 452-454, 1963.
12. Zhu, W-Z.; Biber, B.; Laflamme, MA. *et al.* “Methods for the Derivation and Use of Cardiomyocytes from Human Pluripotent Stem Cells.” Totowa, NJ: Humana Press; 2011.
13. Yu ,J.; Vodyanik, MA.; Smuga-Otto, K. *et al.* “Induced pluripotent stem cell lines derived from human somatic cells.” *Science.* Vol. 318, pp. 1917-1920, 2007.
14. Shiba, Y.; Fernandes, S. *et al.* “Human ES-cell-derived cardiomyocytes electrically couple and suppress arrhythmias in injured hearts.” *Nature Letter.* 2012.
15. Zhang, D; Shadrin, IY *et al.* “Tissue-engineered cardiac patch for advanced functional maturation of human ESC-derived cardiomyocytes.” *Biomaterials.* Vol. 34, no. 23, pp. 5813-5820, 2013.

16. Kim, D-H,;Kshitiz, *et al.* “Nanopatterned cardiac cell patches promote stem cell niche formation and myocardial regeneration.” *Integrative Biology (Camb).* Vol. 4, pp. 1019–1033, 2012.
17. Bursac, N.; Leong, K. *et al.* "Novel anisotropic engineered cardiac tissues: Studies of electrical propagation." *Biochem Bioph Res Co.* Vol. 361, no. 4, pp. 847-853, 2007.
18. W.-H. Zimmermann *et al*. "Engineered heart tissue grafts improve systolic and diastolic function in infarcted rat hearts." *Nature Medicine.* Vol. 12, no. 4, pp. 452-458, 2006.
19. Bowers, S.L.K.; Banerjee, I. *et al.* “The extracellular matrix: At the center of it all.” *Journal of Molecular and Cellular Cardiology.* Vol. 48, no. 3, pp. 474-482, 2010.
20. Hinds, S. *et al*. “The role of extracellular matrix composition in structure and function of bioengineered skeletal muscle.” *Biomaterials*. Vol. 32, no. 14, pp. 3575-3583, 2011.
21. Zile, M.R. “New Concepts in Diastolic Dysfunction and Diastolic Heart Failure: Part II: Causal Mechanisms and Treatment.*” Circulation*. Vol. 105, no. 12, pp.1503-1508, 2002.
22. Bosman, F.T.; Stamenkovic, I.. “Functional structure and composition of the extracellular matrix.” *The Journal of Pathology*. vol. 200, no.4, pp. 423-428, 2003.
23. Kim, D.-H.; Lipke, E. *et al*. "Nanoscale cues regulate the structure and function of macroscopic cardiac tissue constructs." *Proceedings of the National Academy of Sciences of the United States of America.* Vol. 107, no. 2, pp. 565-570, 2010.
24. Kim, D.-H.; Lee, H. *et al.* “Biomimetic Nanopatterns as Enabling Tools for Analysis and Control of Live Cells.” *Advanced materials.* 2010.
25. Wang, Peng-Yuan; Thissen, Helmut *et al.*, “The roles of RGD and grooved topography in the adhesion, morphology and differentiation of C2C12 Skeletal Myoblasts.” *Biotechnology and Bioengineering.* Vol. 109, no. 8, pp. 2104-2115, 2012.
26. Le Saux, Guillaume; Magenau, Astrid *et al*. “The relative importance of topography and RGD ligand density for endothelial cell adhesion.” *PLOS One.* Vol. 6, no. 7, pp. 1-13, 2011.
27. Tulloch, NL; Muskheli, V *et al.* “Growth of engineered human myocardium with mechanical loading and vascular coculture.” *Circulation Research.* Vol. 109, no. 1, pp. 47-59, 2011.
28. Wang, Peng-Yuan; Yu, Jiashing *et al.* “Modulation of alignment, elongation and contraction of cardiomyocytes through a combination of nanotopography and rigidity of substrates.” *Acta Biomaterialia.* pp. 1-9, 2011.

29. Engler, Adam J.; Carag-Krieger, Christine *et al.* “Embryonic cardiomyocytes beat best on a matrix with heart-like elasticity: scar-like rigidity inhibits beating.” *Journal of Cell Science.* Vol. 121, pp. 3794-3802, 2008.
30. Ghassemi, Saba; Meacci, Giovanni *et al.* “Cells test substrate rigidity by local contractions on submicrometer pillars.” *Proceedings of the National Academy of Sciences of the United States of America.* Vol. 109, no. 14, pp. 5328-5333, 2012
31. Galie, PA; Halid, N *et al.* “Substrate stiffness affects sarcomere and costamere structure and electrophysiological function of isolated adult cardiomyocytes.” *Cardiovascular Pathology.* Vol. 22, no. 3, pp. 219-229, 2012.
32. W.-H. Zimmermann *et al*. "Tissue engineering of differentiated cardiac muscle construct." *Circulation Research.* Vol. 90, no. 2, pp. 223-230, 2002.
33. M. Radisic, H. Park and *et. al*. "Functional assembly of engineered myocardium by electrical stimulation of cardiac myocytes cultured on scaffolds." *Proceedings of the National Academy of Sciences of the United States of America.* Vol. 101, no. 52, pp. 18129-34, 2004.
34. Kim, Hong Nam; Kang, Do-Hyun *et al.* “Patterning Methods for Polymers in Cell and Tissue Engineering.” *Annals of Biomedical Engineering.* Vol. 40, no.6, pp. 1339-1355, 2012.
35. J. Jacot, A. McCulloch and J. Omens. "Substrate stiffness affects the functional maturation of neonatal rat ventricular myocytes." *Biophysiology Journal.* Vol. 95, no. 7, pp. 3479-3487, 2008.
36. Jacot, Jeffrey G.; Kita-Matsuo, Hiroko *et al.* “Cardiac myocyte force development during differentiation and maturation.” *Annals of the New York Academy of Sciences.* Vol. 1188, pp. 121-127, 2010.
37. Al-Haque, Shahed; Miklas, Jason W. *et al.* “Hydrogel Substrate Stiffness and Topography Interact to Induce Contact Guidance in Cardiac Fibroblasts.” *Macromolecular Bioscience.* Vol. 12, no. 10, pp. 1342-1353, 2012.
38. Kuo, PL; Lee, H *et al.* “Myocyte shape regulates lateral registry of sarcomeres and contractility.” *American Journal of Pathology.* Vol. 181, no.6, pp. 2030-2037, 2012.
39. Laflamme, MA and CE Murry. “Heart regeneration.” *Nature.* Vol.473, pp. 326–335, 2010.
40. Boyle, AJ, SP Schulman *et al.* “Is stem cell therapy ready for patients? Stem Cell Therapy for Cardiac Repair. Ready for the Next Step.” *Circulation.* Vol. 114, pp. 339–352. 2006.

41. Sparrow, JC and F Schöck. “The initial steps of myofibril assembly: integrins pave the way.” *Nature Review Molecular Cell Biology.* Vol. 10, pp. 293–298. 2009.
42. Riehl, B; Park, J. *et al.* “Mechanical Stretching for Tissue Engineering: Two-Dimensional and Three-Dimensional Constructs.” *Tissue Engineering: Part B.* Vol. 18, no. 4. 2012
43. Hollweck, T.; Akra, B. *et al.* “A Novel Pulsatile Bioreactor for Mechanical Stimulation of Tissue Engineered Cardiac Constructs”. *Functional Biomaterials.* 2011.
44. N. Bursac *et al*. "Cardiac muscle tissue engineering: toward an in vitro model for electrophysiological studies." *American Journal of Physiology - Heart and Circulatory Physiology.* Vol. 277, no. 2, pp. H433-H444, 1999.
45. Boheler, K. R. *et al.* "Differentiation of Pluripotent Embryonic Stem Cells into Cardiomyocytes." *Circulation Research.* Vol. 91, no. 3, pp. 189-201, 2002.
46. Dvir, T.; Timko, B. P. *et al*. “Nanowired Three-Dimensional Cardiac Patches.” *Nature Nanotechnology*. Vol. 6, pp. 720-725, 2011.
47. Hollweck, T.; Akra, B. *et al.* “A Novel Pulsatile Bioreactor for Mechanical Stimulation of Tissue Engineered Cardiac Constructs.” *Functional Biomaterials.* 2011.
48. Shimko, V.; Claycomb, W. “Effect of Mechanical Loading on Three-Dimensional Cultures of Embryonic Stem Cell-Derived Cardiomyocytes. *Tissue Engineering.* Vol. 14, no. 1, pp. 49-58, 2008.
49. McNamara, L. E.; McMurray, R. *et al*. "Nanotopographical Control of Stem Cell Differentiation." *Journal of Tissue Engineering.* pp. 1-14, 2010.
50. Spach, MS.; Heidlage, JF. *et al*. “Cell size and communication: Role in structural and electrical development and remodeling of the heart.” *Heart rhythm: the official journal of the Heart Rhythm Society*. Vol.1, pp. 500-515, 2004.
51. Gherghiceanu, M.; Barad, L. *et al.* “Cardiomyocytes derived from human embryonic and induced pluripotent stem cells: Comparative ultrastructure.” *Journal of cellular and molecular medicine*. Vol. 15, pp. 2539-2551, 2011.
52. Snir, M.; Kehat, I. *et al.* “Assessment of the ultrastructural and proliferative properties of human embryonic stem cell-derived cardiomyocytes.” *American journal of physiology. Heart and circulatory physiology*. Vol. 285, pp. H2355-2363, 2003.
53. Dolnikov, K.; Shilkrut, M. *et al*. “Functional properties of human embryonic stem cell-derived cardiomyocytes: Intracellular ca2+ handling and the role of sarcoplasmic reticulum in the contraction”. *Stem cells*. Vol. 24, pp. 236-245, 2006.

54. Heidi Au, HT.; Cui, B. “Cell culture chips for simultaneous application of topographical and electrical cues enhance phenotype of cardiomyocytes.” *Lab on a chip*. Vol. 9, pp. 564-575, 2009.
55. Lahmers, S.; Wu, Y. *et al*. “Developmental control of titin isoform expression and passive stiffness in fetal and neonatal myocardium.” *Circulation research*. Vol. 94, pp. 505-513, 2004.
56. Snir, M.; Kehat, I. *et al.* “Assessment of the ultrastructural and proliferative properties of human embryonic stem cell-derived cardiomyocytes.” *American journal of physiology. Heart and circulatory physiology*. Vol. 285, pp H2355-2363, 2003.
57. Ziman, AP.; Gomez-Viquez, NL. *et al.* “Excitation-contraction coupling changes during postnatal cardiac development.” *Journal of molecular and cellular cardiology.* Vol. 48, pp. 379-386, 2010.
58. Chen, HS.; Kim, C. *et al.* “Electrophysiological challenges of cell-based myocardial repair.” *Circulation*. Vol. 120, pp. 2496-2508, 2009.
59. Lopaschuk, GD.; Jaswal, JS. “Energy metabolic phenotype of the cardiomyocyte during development, differentiation, and postnatal maturation.” *Journal of cardiovascular pharmacology*. Vol. 56, pp. 130-140, 2010.
60. Xu, XQ.; Soo, SY. *et al.* “Global expression profile of highly enriched cardiomyocytes derived from human embryonic stem cells.” *Stem cells*. Vol. 27, pp. 2163-2174, 2009.
61. Liu, J.; Sun, N. *et al.* “Atomic force mechanobiology of pluripotent stem cell-derived cardiomyocytes.” *PloS one*. Vol. 7, pp. e37559, 2012.